HHS Public Access

Author manuscript

ACS Nano. Author manuscript; available in PMC 2021 August 25.

Published in final edited form as:

ACS Nano. 2020 August 25; 14(8): 9408–9422. doi:10.1021/acsnano.0c05215.

Engineering Plasmonic Nanoparticles for Enhanced Photoacoustic Imaging

Yash Mantri,

Department of Bioengineering, University of California, San Diego, La Jolla, California 92093, United States;

Jesse V. Jokerst

Department of NanoEngineering, Materials Science Program, and Department of Radiology, University of California, San Diego, La Jolla, California 92093, United States;

Abstract

Photoacoustic (PA) imaging is an emerging imaging modality whereby pulsed laser illumination generates pressure transients that are detectable using conventional ultrasound. Plasmonic nanoparticles such as gold nanorods and nanostars are often used as PA contrast agents. The thermoelastic expansion model best describes the PA response from plasmonic nanoparticles: Light absorption causes a small increase in temperature leading to thermoelastic expansion. The conversion of optical energy into pressure waves (p_0) is dependent on several features: (i) the absorption coefficient (μ_a), (ii) the thermal expansion coefficient (β), (iii) specific heat capacity (C_p) of the absorbing material, (iv) speed of sound in the medium (c), and (v) the illumination fluence (F). Controlling the geometry, composition, coatings, and solvents around plasmonic nanostructures can help tune these variables to generate the optimum PA signal. The thermoelastic expansion model is not limited to plasmonic structures and holds true for all absorbing molecules. Here, we focus on ways to engineer these variables to enhance the PA response from plasmonic nanoparticles.

Graphical Abstract

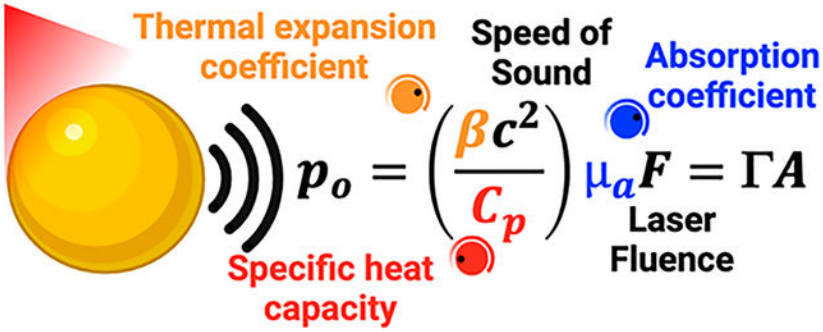

Corresponding Author: Jesse V. Jokerst – Department of NanoEngineering, Materials Science Program, and Department of Radiology, University of California, San Diego, La Jolla, California 92093, United States; jjokerst@ucsd.edu.

Complete contact information is available at: https://pubs.acs.org/10.1021/acsnano.0c05215

The authors declare no competing financial interest.

Keywords

plasmonic nanoparticles; photoacoustic imaging; gold nanoparticles; coatings; enhancement; absorption coefficient; Grüneisen parameter; thermoelastic expansion

Conventional optical imaging uses a light in–light out approach, which limits depth penetration due to scattering in tissue. Ultrasound imaging uses a sound in–sound out approach, which reduces scattering but lacks the spectral capabilities and high contrast of optical imaging. Photoacoustic (PA) imaging solves these limitations and provides spectral ultrasound imaging based on varying optical absorption. PA uses a light in–sound out approach, where pulsed light is absorbed to generate pressure transients that are detectable by ultrasound.[1,2]

PA imaging benefits from contrast agents that produce signal with different characteristics compared to the background. The most commonly used endogenous contrast agents are oxygenated and deoxygenated hemoglobin and melanin.[2,3] Oxy- and deoxyhemoglobin have distinct absorption spectra. Thus, PA signals obtained at different wavelengths can be unmixed to quantify blood oxygen saturation—a key parameter for diagnostics.[4] Exogenous contrast agents with different optical properties can increase contrast and can be engineered as activatable sensing and therapeutic platforms. These exogenous contrast agents range from dyes[5–7] and small molecules[8–10] to nano-[11–13] and microparticles.[14–17] Engineering highly efficient contrast agents can increase sensitivity, image quality, and early stage diagnostics; it can improve therapeutic efficiency.

To design efficient contrast agents, it is important to understand the method of signal generation, of which there are four primary mechanisms: thermal or thermoelastic expansion, vaporization,[15,18,19] optical breakdown, and photochemical processes.[20] For biomedical applications and contrast agent development, we are usually interested in the thermoelastic expansion route, because it does not change or break the properties of the biological sample under observation.[1] Herein, light absorption causes a small increase in temperature (in the milli-Kelvin range), leading to the brief expansion of the contrast agent.[1,20,21] This creates a pressure transient that can be detected acoustically. There is no bulk heating of the medium, because the expansion is spatially and thermally confined using light pulses shorter than the thermal relaxation time of the absorber.[22] The resulting PA signal is a function of the optical, thermal, and elastic properties of the sample.

The pressure difference generated due to thermal expansion (ρ_o) is given below in eq 1.[1] Here, β is the thermal expansion coefficient of the absorbing material in K^{-1}; c is the speed of sound in ms^{-1} in the medium; C_p is the specific heat capacity of the absorber in J/(K kg); μ_a is the absorption coefficient in cm^{-1}; and F is the irradiation fluence in J/cm^2. Γ is the Grüneisen parameter (eq 2) characterizing the thermoacoustic conversion efficiency, and A is the local energy deposition density in J/cm^3 (eq 3).

$$\rho_o = \left(\frac{\beta c^2}{C_p}\right)\mu_a F = \Gamma A \quad (1)$$

$$\Gamma = \left(\frac{\beta c^2}{C_p}\right) \quad (2)$$

$$A = \mu_a F \quad (3)$$

Plasmonic nanoparticles make good photoacoustic contrast agents because of their high absorption cross section, relative inertness, high stability, and a tunable localized surface plasmon resonance (LSPR).[23,24] Gold (spheres, rods, plates, shells, stars) and other metal nanostructures are particularly common as PA contrast agents. They are easily functionalized and can respond to specific chemical cues.[25,26]

To enhance PA signal generation from plasmonic nanoparticles, researchers have turned a few "knobs" as described in eq 1. The illumination fluence (F) is not a nanoparticle property and can be tuned separately, *e.g.*, by laser power. The speed of sound (c) is a function of the tissue type and can be difficult to manipulate externally. However, the absorption coefficient (μ_a), thermal expansion coefficient (β), and specific heat capacity of the absorber (C_p) can be tuned by modifying the nanoparticle shape, material, solvent, and so on. eq 1 can be applied to all absorbing molecules such as endogenous hemoglobin and melanin and is not just limited to plasmonic nanostructures.[1] Here, we review how the nanoparticle properties can be engineered to enhance PA signal (ρ_0). We focus on the thermoelastic expansion model of PA generation and review ways to engineer the variables presented in eq 1.

ABSORPTION COEFFICIENT (μ_A)

The absorption coefficient describes how well a material absorbs incident photons at a defined wavelength—it is directly proportional to photoacoustic signal. As light traverses through a sample, it is either scattered or absorbed. Scattering and absorption is strong in tissues; hence, optical imaging techniques have limited depth penetration (approximately 100 μm). The reduced scattering coefficients for soft tissue and water from 600 to 900 nm range from 10 to 20 cm^{-1} and to less than 0.003 cm^{-1}, respectively. The absorption coefficient ranges from 0.1 to 0.5 cm^{-1} and 0.0015–0.067 cm^{-1}, respectively.[27,28] For PA signal generation, the excitation light must be absorbed to induce thermoelastic expansion (eq 1). A high μ_a produces a high PA signal (eq 1), and there are various ways to increase the absorption coefficient of nanoparticles: increasing absorbance at a wavelength of interest, plasmon coupling leading to local-field enhancement and spectral shifts, and shape control of nanoparticles.

INCREASING ABSORBANCE

Absorbance measures light attenuation through a sample. It combines the effects of photon absorption and scattering. Increased absorption and reduced scattering increase the absorption cross section of a particle. The absorption cross section is the probability that a photon of a particular wavelength is absorbed by a particle. Typical values for nanoparticles range from 2.9 to 33.5 × 10^{11} cm^2.[29] Nanoparticles are employed as PA contrast agents

because of their high absorption cross section compared to that of other small molecules.[30] Generally increasing the absorbance leads to an increase in photoacoustic signal.[31–34] Coatings like polydopamine,[35,36] melanin,[37] titanium dioxide,[38] graphene oxide,[39] and reduced graphene oxide[40,41] on gold nanoparticles increase the absorbance and subsequent PA amplitude. Although uncoated nanoparticles and coatings alone showed no enhancement in all these reports, they do not show if a mixture of the core and shell materials leads to PA enhancement. An example was reported by Leng *et al.* in 2018; they engineered gold nanorod–copper sulfide heterostructures with enhanced photothermal conversion efficiency and photostability.[42] They showed that depositing Cu_7S_4 on gold nanorod tips instead of a uniform shell around a nanorod core reduced scattering and increased absorption (Figure 1a–e). The increased absorption led to a 62% increase in photothermal efficiency. Its effect on PA signal generation remains to be seen.

Adding dyes like rhodamine B,[43] indocyanine green,[44–46] cyanine 5.5, methylene blue, and quenchers like QSY_{21} to nanoparticles like gold or single walled carbon nanotubes increase absorption and enhance PA signals up to 100-fold.[47,48] Upon irradiation, electrons excited to a higher energy state can relax back to their ground state by (i) a nonradiative pathway or vibrational relaxation, (ii) a radiative pathway or fluorescence, or (iii) intersystem crossing or phosphorescence. Maximizing nonradiative relaxation increases PA amplitude, as more energy is converted to heat and thermoelastic expansion.[49]

PLASMON COUPLING LEADING TO LOCAL-FIELD ENHANCEMENT AND SPECTRAL SHIFTS THAT CHANGE μ_A

Individual plasmonic oscillations on noble metal nanostructures can be coupled when nanoparticles are in close proximity to each other.[50] Plasmonic coupling can cause the electric field in the interparticle gap to be boosted by several orders of magnitude, which far exceeds the field enhancement for a single plasmonic nanoparticle (Figure 2a,b).[51–55] The plasmon modes of close particles can either be in phase or out of phase with each other. This causes attraction or repulsion leading to a decrease (red-shift) or an increase (blue-shift) in the hybridized plasmon resonance.[56] Usually, a decrease in nanoparticle size causes a blue-shift, whereas an increase in size due to nucleation or aggregation causes a red-shift.[57] A red-shifted LSPR increases μ_a in the near-infrared (NIR) range, which is favorable for PA imaging. The magnitude of the plasmon shift depends on the particle geometry, plasmon resonance of individual particles, and the interparticle spacing.[52,58]

PA enhancement due to plasmonic coupling has been extensively reported over the years. Gold nanoparticle strings,[59] biodegradable gold nanovesicles,[60] self-assembled semiconducting gold nanoparticles,[61] aggregated gold–silica Janus nanoparticles,[62] and many more examples show that plasmonic coupling between two or more nanoparticles shifts the LSPR into the biological optical window (650–900 nm). Increasing absorbance in the NIR range results in PA enhancement compared to uncoupled controls. Lu *et al.* reported a clever method for plasmon-coupling-related PA enhancement:[63] They manipulated the LSPR band of AuNPs by enzymatic hydrolysis and induced self-assembly of nanoparticles. Nanoparticle assemblies responded to specific enzymatic cues (collagenase IV, Figure 2e)

and self-assembled via hydrogen bonding, π–π stacking, and hydrophobic interactions. Self-assembly of AuNPs resulted in a red-shifted absorption spectrum due to plasmon coupling. The increase in absorbance in the NIR range (680–800 nm) along with thermal overlap of assembled particles resulted in 2-fold enhancement in PA intensity (Figure 2c–e).

Recently, our group reported iodide-doped silver-coated gold nanorods as an activatable PA contrast agent to measure oxidative stress.[13] We showed that the absorption spectra of gold nanorods (AuNRs) can be blue-shifted when coated with increasing amounts of silver (Figure 3a). Blue-shifting of the absorbance reduces μ_a in the NIR range and the PA response at 680 nm. Selective etching of the silver iodide shell using reactive oxygen and nitrogen species can recover the absorption spectra and μ_a of the bare AuNRs (Figure 3b). The increase in μ_a at 680 nm resulted in a 70% increase in the PA intensity in a mouse model of zymosan induced oxidative stress (Figure 3c,d).

SHAPE AND SIZE CONTROL

Optimizing the geometry of plasmonic nanoparticles can significantly affect their optical and photoacoustic properties.[64] Gold nanoparticles are the most commonly used plasmonic PA contrast agents.[65] They can be synthesized as spheres,[66] cubes,[67] plates,[68] rods,[12,13,69–71] cages,[72–74] shells,[75] bipyramids,[76] and stars.[77,78] The tips and edges lead to enhancement of the electromagnetic field as electron density increases at the tips. Simulations have shown that sharper tips have a higher μ_a compared to rounded tips.[79] The emergence of hotspots where plasmons relax thermally via electron–phonon coupling can help generate the PA signal. Electron–phonon coupling describes the movement of atoms in a crystal lattice due to electron oscillations.[80–82] Various shapes exhibit different ratios of absorption and scattering, so some shapes are better suited for PA than others. Gold nanospheres are easy to synthesize, but their LSPR (~530 nm) lies outside the biological optical window.

Gold nanorods are the most widely used PA contrast agents because of their easily tunable absorption spectrum; unfortunately, they are fairly unstable under high fluence laser illumination.[83] Gold nanocages and nanoshells are also applied as biomedical PA contrast agents. Chigrin and co-workers modeled and showed that the most promising geometries are high aspect ratio gold nanorods and gold nanostars with high absorption and low scattering coefficients.[84] Knights *et al.* showed that 40–50 nm AuNRs produced the highest PA signal but were also cytotoxic; 10 nm AuNRs were efficient photoacoustic converters at equivalent total mass showing 2.5-fold PA enhancement.[85] There is a considerable amount of data on how PA is affected by shape and size of gold nanoparticles, but a comprehensive model that can predict PA response from other plasmonic geometries is still missing.

MOVING PLASMONICS INTO THE SECOND NEAR-INFRARED WINDOW (1000–1700 NM)

Until recently, the field has devoted most of its efforts into engineering plasmonic nanostructures that operate within the first biological optical window (600–900 nm). There exists a second NIR window (1000–1700 nm) where biological tissues have low background. Designing contrast agents that operate within this range can help image deeper

by reducing scattering from tissue. Illumination fluence (F) can be increased when using longer (less energetic) wavelengths, which is governed by the maximum permissible exposure limit. Although water absorbs strongly at 1450 nm, researchers have shown promising results by moving plasmonics into the NIR-II window. Most of the work in this area is around semi-conductor-based polymeric nanoparticle assemblies with broadband absorption.[86–88] Recently, Chen *et al.* reported a miniaturized gold nanorod for photoacoustic imaging in the NIR-II window.[89] The LSPR peak of gold nanorods is controlled by the nanoparticle's aspect ratio. Increasing the aspect ratio red-shifts the LSPR of nanorods. Aspect ratios of 6 or higher can push the LSPR into the NIR-II range. The common seed-mediated synthesis of high aspect ratio gold nanorods results in particles that absorb in the NIR-II range but have large dimensions (120 × 18 nm).[71,89] But for *in vivo* applications, nanoparticles must be less than 100 nm in size to favor extravasation and accumulation in tumors. Chen and co-workers synthesized high aspect ratio gold nanorods (49 × 8 nm) using a seedless synthesis process.[89] The resulting nanoparticles showed peak absorbance at 1064 nm and 3.5-fold photoacoustic enhancement. PA signal from miniaturized nanorods was higher due to a higher surface-area-to-volume ratio compared to their larger counterparts.

The absorption coefficient of plasmonic nanostructures can be easily tuned via the material properties or shape of the nanostructure.[90] For enhanced PA, the ideal nanoparticle should have high light absorbance and low scattering properties. Nanoparticle geometry and size have a significant impact on its optical properties. Geometries with sharp tips such as nanostars exhibit localized plasmon hotspots that result in a higher μ_a. Moving plasmonics into the NIR-II window can help image deeper within tissues. The use of longer and lower energy wavelengths will aid in the clinical translation of PA by keeping exposure levels under the maximum permissible exposure limit while still providing sufficient imaging signal.

Another example was demonstrated by Wang *et al.* in 2014.[91] Using FDTD simulations, they modeled "rod-in-shell" nanoparticles with absorption in both the NIR-I and II windows (Figure 4). Their model nanoparticle had a gold core (60 × 20 nm), a composite Ag/Au (1:1) outer shell (4 nm), and a hollow gap in between (5 nm) (Figure 4c). Under longitudinal excitation mode, their nanoparticle showed two distinct absorption peaks at 681 and 1158 nm, respectively (Figure 4d). This was attributed to near-field enhancement and plasmon hybridization between the core and shell layers. With a higher absorption cross section compared to uncoated gold nanorods, these rod-in-shell particles could show high efficiency in both PA and photothermal therapy (PTT) applications.

Broadening the absorbance of gold nanoparticles into the NIR-II range via shape control, gold nanoechinus[92] or with coatings, or polydopamine blackbody[36] have been reported. As described earlier, plasmonic coupling of nanoparticles due to self-assembly or aggregation can also red-shift its absorbance spectra. The red-shift can be engineered into the NIR-II range. Overall, the high absorption cross section, tunability, and sensitivity of plasmonic nanoprobes along with the ability to image deeper and with higher fluence make their move into the second biological optical window highly desirable.[49,93] Since most of the work done

in this field is based on semiconducting and organic probes, plasmonics remains a relatively new but extremely promising area of study.

THERMAL EXPANSION COEFFICIENT (β)

The thermal expansion coefficient describes how the size of an object changes as a function of temperature. The thermal expansion coefficient is a material property and hence very difficult to change in a nanoparticle. To the best of our knowledge, there have been no reports of engineering the thermal expansion coefficient of a nanoparticle. However, many groups have modeled and partially shown that the PA signal is a summed contribution of the thermal expansion of the nanoparticle and its solvent. During a laser pulse, heat cannot be completely confined within the nanoparticle—some of it diffuses into the solvent, leading to a shell-like layer of the solvent around the nanoparticle with elevated temperature. The resulting temperature increase induces thermal expansion in both the nanoparticle and the solvent (Figure 5). The amount of heat transferred into the solvent depends on the length of the laser pulse, interfacial thermal resistance (Kapitza resistance) at the nanoparticle–solvent interface, and the thermoelastic properties of the solvent itself.[94] Hence, tuning the solvent properties can enhance the PA signal.

The PA varying response of silica-coated gold nanospheres in water, silicone oil, and toluene was reported in 2012 by Chen *et al.*[94] They showed that the PA signal is proportional to the temperature-dependent Grüneisen parameter (eq 2) of the respective solvent (Figure 6). Ethanol has a much higher β and a much lower specific heat capacity (C_p) compared to water at room temperature.[95] Hence, the Grüneisen parameter (eq 2) for ethanol is 11.7-fold greater than that of water at room temperature.[95] Shi *et al.* modeled and experimentally showed that changing the solvent from water to ethanol for gold nanospheres resulted in a 4.5-fold higher PA signal.[95] Furthermore, coating gold nanospheres with a shell having a higher thermoacoustic conversion efficiency than water could enhance the PA signal. The β for PDMS is 4.5-fold higher than that of water. By confining the heat distribution within the PDMS shell, a 3.5-fold PA enhancement was observed by Shi *et al.*[95]

Emelianov and others have modeled shown that over 90% of the PA signal is generated within the solvent compared to the absorbing nanoparticle.[94–96] The optical energy absorbed by the nanoparticle diffuses into the solvent as heat because of the small size of nanoparticles (high surface-area-to-volume ratio). The intensity of the PA signal is proportional to the outgoing heat flux.[94] Water is an ideal solvent to study the PA response of a nanoparticle. The thermal expansion of water disappears at 3.98 °C as water is densest at that temperature; hence, any PA signal generated from the heating solvent vanishes, but the PA generated from the nanoparticle can still be transmitted.[94]

Coatings such as silica,[97–99] reduced graphene oxide,[40] and zinc tera(4-pyridyl)porphyrin[100] can change the Kapitza resistance or thermal conductance at the nanoparticle–solvent interface, leading to PA enhancement. In the thermoelastic expansion model of PA, each nanoparticle has its own thermal profile: the particle itself and the heated solvent around it (Figure 5). When aggregated, the thermal profiles of individual nanoparticles can overlap and collectively add to increase the rate of heat flux into the solvent.[101] This was

demonstrated by Bayer et. al in 2013.[102] PA signal from aggregated silica-coated gold nanoparticles was up to 7-fold higher compared to dispersed silica-coated gold nanoparticles. A 25 nm thick silica shell around gold nanorods measuring 65 × 12 nm in size ensured that there was no plasmonic coupling between aggregated nanoparticles (Figure 7a,b). *In vitro* tests showed that PA signal linearly increased as a function of particle concentration (Figure 7c,d).

Another example was demonstrated by Chen *et al.* in 2017; here, they synthesized temperature sensitive poly(*N*-isopropy-lacrylamide) (PNIPAM) nanoparticles loaded with gold nanorods or copper sulfide nanospheres.[103] PNIPAM shrinks above its lower critical solution temperature (LCST) at 32 °C. The gold nanorods or copper sulfide nanospheres were drawn closer together as the temperature increased above 32 °C—this increased the thermal flux from the cluster into the surrounding medium. Using this dynamic nanogel, they were able to enhance the PA signal from gold nanorods and copper sulfide nanospheres up to 22- and 30-fold, respectively (OD = 3.33 for 1 cm optical path length). Even below the LCST, PNIPAM–AuNR showed a 3.5-fold PA enhancement versus pure AuNR solution, which was attributed to random thermal overlap of nanoparticles within the gel matrix. PNIPAM–CuS showed no change in optical absorption due to aggregation but showed a 5.5-fold PA enhancement above the LCST. This confirmed that enhancement was due to thermodynamic and not plasmonic coupling effects.

The PA signal generated from core–shell nanoparticles, specifically gold–silica core–shell nanostructures, has been studied and modeled extensively. There are conflicting reports that show both PA enhancement (up to 3-fold for AuNRs)[94,97,98,104,105] and a PA decrease[106] upon silica coating. The most comprehensive model in this field was recently reported by Shahbazi *et al.* in 2019.[96] This group modeled the heat transfer and PA signal generation from a core–shell gold nanosphere using a nanosecond pulsed laser illumination. They considered the interfacial thermal resistance at the core–shell and shell–solvent interface and the temporal waveform of the laser pulse and showed that both parameters had a dramatic impact on PA amplitude. They also showed that only 7% of the PA signal is generated within the nanoparticle and that the fluid-generating region is a spherical shell almost twice as thick as the radius of the nanoparticle.

Other groups have looked at the ideal core–shell sizes and reported various values. Chen *et al.* observed the highest PA response from 13 nm gold cores coated with 18 nm silica shells.[94] Kumar *et al.* reported 6-fold enhancement using 35 nm gold cores coated with 20 nm silica shells.[105] Both groups reported that increasing the shell thickness above a certain value results in loss of PA signal as the thermal energy is confined within the shell and does not diffuse into the solvent. Using thin shells with short duration laser pulses result in the highest amplification.

On the contrary, Pang *et al.* reported that the Kapitza resistance has negligible effect on PA signal generation and silica coating causes a reduction in PA amplitude.[106] For uncoated gold nanospheres under 5 ns pulsed illumination, the Kapitza resistance had a negligible effect on PA amplitude. To see the effects of Kapitza resistance, they dropped the pulse duration to 0.1 ns. They assume that the Kapitza resistance at the shell–water interface is

within the same order of magnitude as the uncoated control. The thermal conductivity of gold (314 W/m K) is much higher than that of silica (0.2 W/m K). Others have shown that the rate of heat dissipation is approximately 1.6-fold faster for silica-coated gold nanoparticles compared to uncoated controls, and hence, the Kapitza resistance should be different for the two as well.[107]

Engineering the thermal expansion coefficient of a nanoparticle has yet to be reported. Most (>90%) of the PA response is generated by the solvent around the nanoparticle, and thus, choosing a solvent with a high β can significantly enhance the PA response; however, this is not always possible in biological applications. The Kapitza resistance can be tuned to maximize the thermal energy transfer from the nanoparticle to its solvent. Thin silica coatings that reduce the Kapitza resistance have shown promise in this direction.

SPECIFIC HEAT CAPACITY (C_P)

The specific heat capacity is the amount of thermal energy required to raise the temperature of a substance per unit of mass. Photoacoustic calorimetry is often used to measure the thermal properties of materials.[108] To the best of our knowledge, there is no reported example of engineering the specific heat capacity of a nanoparticle to tune the PA response. Alloying metals can result in a new specific heat capacity compared to individual metals. Although there is no reported example of engineering the specific heat capacity of a nanoparticle, there is an example of alloyed Au–Ag nanoparticles that lead to PA enhancement. Hatef *et al.* reported that PA signals from Au–Ag alloyed nanoparticles were up to 2.5- and 10-fold higher compared to only gold or silver nanoparticles, respectively.[109] They attributed this enhancement to an increased absorption cross section and did not investigate the effects of alloying on the specific heat capacity of the particle. It would be interesting to study the effect of alloying and changing the specific heat capacity of nanoparticles to engineer a desired PA response.

LASER FLUENCE (F)

Fluence is defined as the laser pulse energy (J) incident on the effective focal spot (cm^2). Laser pulse energy is a function of optical power and the pulse width (usually nanosecond scale). Laser fluence is an externally controlled variable as described in eq 1. Various groups have reported optimal laser configurations to obtain the maximum PA generation. The nonlinear increase in PA intensity as a function of laser fluence is widely reported for gold nanoparticles. The nonlinearity is usually attributed to changes in thermophysical parameters due to a localized increase in temperature at higher laser fluences.[110] Increasing the pulse width also increases the laser fluence, causing the PA signal to increase as long as thermal confinement is met. PA intensity usually plateaus at longer pulse widths.[95]

More recently, groups have reported femtosecond pulsed irradiation for PA imaging. Although laser fluence under fs pulses is lower, groups have found ingenious ways to enhance PA and thermal stability.[111] Femtosecond pulses can allow for two-photon photoacoustics using longer wavelengths and increasing depth penetration.[112] Masim *et al.* reported PA enhancement from gold nanoparticles using a pair of time-delayed femtosecond

pulses (pulse width = 40 fs and E_p = 0.1 mJ).[113] They studied photoacoustic intensity as a function of time delay between two pulses from 0 to 15 ns and showed that PA increased from 0 to 15 ns. They also showed that enhancement was maximized when the first pulse was 20–30% of the total energy delivered. The first pulse primed the solution for bubble generation (cavitation), while the second pulse was used to acquire the PA response (2-fold higher). Laser pulses with sharper temporal waveforms produce PA signals that are more sensitive to environmental changes (such as thermal resistance) and thus increase the probability of signal amplification.[96] Contrast agents that excite at the same wavelength but emit PA signal at various ultrasound frequencies could also help in multiplexing and sensing applications.

The laser fluence is a key parameter to obtain relevant PA signal. It is important to keep the laser fluence under the maximum permissible exposure limit (typically under 20 mJ/cm^2). The use of femtosecond pulses can generate stronger PA signal via other mechanisms such as cavitation. Although increasing laser fluence can lead to PA enhancement, high fluence illumination can also lead to nanoparticle degradation especially in nonspherical structures.[99]

FUTURE OUTLOOKS

The thermal expansion model of nanoparticle-based photoacoustic signal generation still remains the primary mode to create contrast in biomedical applications. The absorption coefficient (μ_a) is the easiest knob to tune to enhance PA contrast. Increasing the absorbance and reducing scattering using plasmonically coupled heterostructures or by incorporating NIR absorbing dyes can help design more efficient PA contrast agents. Shape control can engineer the local electromagnetic-field enhancement around a nanoparticle, but the field lacks a more comprehensive comparison between different shapes. Nanoparticles that absorb in the second optical window (1000–1700 nm) can help image deeper and reduce scattering.[89] Challenges like the absorption of water (1450 nm) still need to be overcome, but there are significant advances in this area already.[114] Engineering dispersion and shapes of chiral nanoparticles can lead to higher sensitivity in the optical properties (refractive index) of the nanoparticle. Polarization-dependent excitation could offer strong contrast even in highly absorbing media and biological tissues.[115–117] Nanoprobes that change their optical properties in different suspension environments can be excellent sensing platforms. Recently, CuS nanoplates that responded to refractive index changes (160–600 nm RIU^{-1}) in their suspension media with changes in particle diameter and operation wavelength (1100–1250 nm) were reported.[118]

Tuning the thermal expansion coefficient (β) of a nanoparticle is challenging. While phase changing hybrid plasmonic nanoparticles could be promising,[119] there is no such report for PA applications. Most of the PA signal is generated within the solvent, and tuning the rate of heat flux into the solvent is a key parameter to optimize the PA response. Silica-coated gold nanoparticles are the most studied nanosystem in the field, and it may be useful to study other plasmonic-semiconducting nanosystems.

The specific heat capacity (C_p) of a nanoparticle is difficult to engineer, but alloyed nanoparticles with tunable thermophysical properties can further enhance the PA contrast. The laser fluence (F) is a key parameter for good contrast. Anisotropic nanoparticles tend to be unstable under high fluence illumination, because they deform into a more thermodynamically favorable shape. Using femtosecond pulses that enhance contrast via other methods of PA generation is encouraging.

Other ways to enhance PA such as cavitation are promising.[120] Nanoparticle-coated microbubbles have shown up to a 10-fold increase in PA amplitude due to cavitation even at low laser fluences.[15]

Deep-learning tools are usually used to increase PA contrast during image processing.[121] Tools that can model and predict the photoacoustic behavior of various old and novel nanoparticles may benefit the field in the future.

Gold is the most commonly used contrast agent due to its highly tunable optical properties, high photoacoustic conversion efficiency, and relative biological inertness. Of course, other materials can also generate PA signal: polypyrrole-coated iron–platinum[122] and platinum-chelated bilirubin have also been reported[123] with excellent biocompatibility and a strong PA response under 808 nm illumination. Homan *et al.* and others have shown that functionalized silver nanoparticles can be used as a PA sensing platform for a host of biomedical imaging applications.[124,125] Ku *et al.* reported copper sulfide nanoparticles operating in the NIR-II window (1064 nm) as a PA contrast agent. Operating in the NIR-II window, they were able to image ~5 cm deep in chicken breast.[126] Although PA contrast agents other than gold have been reported, an empirical study to compare different nanoplatforms is still missing.

It is important to note that the thermoelastic expansion model of PA generation in eq 1 holds true for all absorbing molecules such as melanin, hemoglobin, and small molecules, not just for plasmonic nanoparticles.[1] A substantial amount of work has been done with nonplasmonic PA contrast agents,[127–129] but more work is required with other plasmonic nanoplatforms.

PLASMONIC STABILITY

Although gold nanorods are widely used as photoacoustic contrast agents, they are plagued with low photothermal stability. The rod structure is thermodynamically unfavorable, leading to nanoparticle reshaping under high fluence illumination. Reducing illumination fluence by using light emitting diodes (LEDs) instead of lasers can offer a cheap and easy solution. LEDs operate well below the MPE, which is the currently holding back the clinical translation of laser-based PA systems. But eq 1 clearly shows that reducing F will also reduce p_o. This may be acceptable if μ_a, β, or C_p are tuned to make a highly efficient contrast agent. Furthermore, two-photon excitation using less energetic and longer wavelengths can improve photostability and depth penetration. Some work on organic polymer–plasmonic and dye–plasmonic hybrid nanostructures has been reported in this space.[43,130,131]

In the advent that low-fluence illumination is not feasible, nanoprobes can also be shielded using coatings to improve their photothermal stability. For gold nanorods, coatings like silica,[99] reduced graphene oxide,[40] and polydopamine[35] have increased photothermal stability. Increasing the surface-area-to-volume ratio of nanoparticles allows faster dissipation of heat into the solvent, which increases PA amplitude and photothermal stability. Miniaturized gold nanorods (48 × 8 nm) show 3-fold higher photothermal stability compared to larger rods with the same aspect ratio (120 × 18 nm).[89] Other materials and morphologies such as palladium nanosheets have also shown enhanced stability, but the tests in this study were carried out at a relatively low fluence of 4 mJ/cm^2.[132] Improving photothermal stability will always be highly sought after, as it allows contrast agents to be imaged for longer time periods. Higher stability can also increase sensitivity and allow longer illumination times, which can improve the efficacy for PTT applications.

MULTIFUNCTIONAL PHOTOACOUSTIC PLASMONIC NANOPROBES

Multifunctional nanoprobes that provide contrast in photoacoustics as well as other imaging modalities are especially helpful. Using proven and standard imaging techniques like magnetic resonance imaging (MRI) and ultrasound, multimodal contrast agents can independently validate the PA response.[12,133,134] This is particularly helpful, since there is no clinically approved photoacoustic imaging system on the market yet. One such triple modal contrast agent was reported by Vijayaraghvan *et al.* in 2016.[92] Here, they synthesized plasmonic gold nanoechinus and used them as upconverting, fluorescent, and photoacoustic contrast agents operating in the NIR-II range. Regura *et al.* reported a Janus plasmonic–magnetic gold–iron oxide nanoparticle that provided contrast with X-ray, CT, T_2- weighted MRI, PA, and dark-field optical microscopy.[135] The ability to multiplex various techniques can help extract maximum information from the probe.

Theranostic nanoprobes that can diagnose and treat a condition are extremely desirable. The ability to sense, activate, and treat can help with targeted drug delivery and improve treatment efficacy. PTT is the most common theranostic application for photoacoustic contrast agents.[136–138] PA contrast agents are ideal for PTT, since they have a high absorption cross section and high photothermal conversion efficiency. Plasmonic nanoparticles can be engineered with molecular beacons that seek out specific diseased sites such as tumors where they are retained through the enhanced permeability and retention (EPR) effect. The increasing concentration of nanoparticles within the tumor microenvironment not only increases PA contrast but also helps in ablating the tumor with PTT.[139–142] Theranostic applications beyond PTT are a relatively new field of study, which is very encouraging. Hybrid plasmonic structures have shown promising results. Recently, our group and others reported a gold–silver hybrid nanoparticle for treatment and photoacoustic imaging of drug resistant bacterial infections.[68,70]

SAFETY AND CLINICAL TRANSLATION

Reducing the cytotoxicity of contrast agents is paramount for successful clinical translation. Gold is a commonly used contrast agent for PA because of its relative biological inertness. However, the both the surface chemistry and the underlying substrate are important. Indeed,

gold nanorods are plagued with cytotoxicity issues because of the cetyltrimethy-lammonium bromide (CTAB) surfactant used during gold nanorod synthesis. CTAB forms a bilayer around the gold nanorod, giving it a high positive charge, keeping it colloidally stable. CTAB can cause defects in the cell membrane, leading to cell death.[143,144] High doses of CTAB are often used as a positive control for cell death in cytotoxicity assays.[13] A substantial body of work has been done to reduce the cytotoxic effects of gold nanoparticles through surface modifications using polyethylene glycol,[145] phosphatidylcholine,[146] bovine serum albumin,[147] poly(acrylic acid), and poly(allylamine) hydrochloride.[144] A comparative study on shape-dependent cytotoxic effects of gold nanoparticles (spheres, rods, and stars) revealed that cytotoxicity was highest in rods followed by stars and nanospheres, respectively.[148] Gold nanoparticles were also found to be more biocompatible (72%) than silver nanoparticles (58%) at 100 μM using HepG2 cells.

The cytotoxicity of plasmonic contrast agents is the biggest hurdle for their clinical translation. Although designing multifunction probes is beneficial for complex sensing and therapeutic applications, it is often accompanied by complex synthesis processes and cytotoxic nanoparticles. Designing simpler yet safer nanoparticles would aid in the quick translation of PA contrast agents into clinics. While others like Halas and West have used plasmonics for photothermal therapy,[149] we are unaware of research groups using plasmonics and PA in humans, but the use of endogenous contrast agents such as melanin[150] and hemoglobin[151] has been reported. Unlike plasmonics, the endogenous nature of these contrast agents means that they cannot be tuned to maximize their PA response. The ability to carefully engineer plasmonic probes to specifically optimize the PA response for various biomedical applications makes them highly desirable.[152,153]

CONCLUSION

Overall, plasmonic nanoparticles can be engineered for photoacoustic imaging by tuning one of the many “knobs” presented in eq 1. The acquired PA signal is a complex response from the nanoparticle, its shell, and the solvent around it. Although other methods of PA enhancement like cavitation are not properly understood, they are still promising. The field will continue to strive toward increasing the biocompatibility and photothermal stability of plasmonic nanostructures. This will facilitate more sensitive contrast agents for clinical translation. Multimodal and multifunctional nanoprobes are an important future research focus for photoacoustics.

ACKNOWLEDGMENTS

The table of contents figure and Figure 5 were created with BioRender.com. We acknowledge support from the National Institutes of Health through DP2 HL137187, HL137187 S1, R21AG065776 and R21DE029025-01.

REFERENCES

(1). Xu M; Wang LV Photoacoustic Imaging in Biomedicine. Rev. Sci. Instrum 2006, 77, No. 041101.
(2). Beard P Biomedical Photoacoustic Imaging. Interface Focus 2011, 1, 602–631. [PubMed: 22866233]

(3). Wang X; Xie X; Ku G; Wang LV; Stoica G Noninvasive Imaging of Hemoglobin Concentration and Oxygenation in the Rat Brain Using High-Resolution Photoacoustic Tomography. J. Biomed. Opt 2006, 11, No. 024015. [PubMed: 16674205]

(4). Hester SC; Kuriakose M; Nguyen CD; Mallidi S Role of Ultrasound and Photoacoustic Imaging in Photodynamic Therapy for Cancer. Photochem. Photobiol 2020, 96, 260–279. [PubMed: 31919853]

(5). Wang J; Jeevarathinam AS; Humphries K; Jhunjhunwala A; Chen F; Hariri A; Miller BR III; Jokerst JV A Mechanistic Investigation of Methylene Blue and Heparin Interactions and Their Photoacoustic Enhancement. Bioconjugate Chem 2018, 29, 3768–3775.

(6). Cheng H-B; Li Y; Tang BZ; Yoon J Assembly Strategies of Organic-Based Imaging Agents for Fluorescence and Photoacoustic Bioimaging Applications. Chem. Soc. Rev 2020, 49, 21–31. [PubMed: 31799523]

(7). Jeevarathinam AS; Lemaster JE; Chen F; Zhao E; Jokerst J Photoacoustic Imaging Quantifies Drug Release from Nanocarriers *via* Redox Chemistry of Dye-Labeled Cargo. Angew. Chem., Int. Ed 2020, 59, 4678–468.

(8). Hariri A; Zhao E; Jeevarathinam AS; Lemaster J; Zhang J; Jokerst JV Molecular Imaging of Oxidative Stress Using an Led-Based Photoacoustic Imaging System. Sci. Rep 2019, 9, 11378. [PubMed: 31388020]

(9). Zhang J; Zhen X; Upputuri PK; Pramanik M; Chen P; Pu K Activatable Photoacoustic Nanoprobes for *In Vivo* Ratiometric Imaging of Peroxynitrite. Adv. Mater 2017, 29, 1604764.

(10). Huang J; Pu K Activatable Molecular Probes for Second Near-Infrared Fluorescence, Chemiluminescence, and Photoacoustic Imaging. Angew. Chem 2020, 132, 11813–11827.

(11). Lemaster JE; Jokerst JV What Is New in Nanoparticle-Based Photoacoustic Imaging? Wiley Interdiscip. Rev.: Nanomed. Nanobiotechnol 2017, 9, No. e1404.

(12). Jokerst JV; Cole AJ; Van de Sompel D; Gambhir SS Gold Nanorods for Ovarian Cancer Detection with Photoacoustic Imaging and Resection Guidance v*ia* Raman Imaging in Living Mice. ACS Nano 2012, 6, 10366–10377. [PubMed: 23101432]

(13). Mantri Y; Davidi B; Lemaster JE; Hariri A; Jokerst JV Iodide-Doped Precious Metal Nanoparticles: Measuring Oxidative Stress *In Vivo via* Photoacoustic Imaging. Nanoscale 2020, 12, 10511–10520. [PubMed: 32396928]

(14). Weber J; Beard PC; Bohndiek SE Contrast Agents for Molecular Photoacoustic Imaging. Nat. Methods 2016, 13, 639–650. [PubMed: 27467727]

(15). Dixon AJ; Hu S; Klibanov AL; Hossack JA Oscillatory Dynamics and *In Vivo* Photoacoustic Imaging Performance of Plasmonic Nanoparticle-Coated Microbubbles. Small 2015, 11, 3066–3077. [PubMed: 25703465]

(16). Shrestha B; DeLuna F; Anastasio MA; Yong Ye J; Brey EM Photoacoustic Imaging in Tissue Engineering and Regenerative Medicine. Tissue Eng., Part B 2020, 26, 79–102.

(17). Upputuri PK; Pramanik M Recent Advances in Photoacoustic Contrast Agents for *In Vivo* Imaging. Wiley Interdiscip. Rev.: Nanomed. Nanobiotechnol 2020, 12, e1618. [PubMed: 32027784]

(18). Meng Z; Zhou X; She J; Zhang Y; Feng L; Liu Z Ultrasound-Responsive Conversion of Microbubbles to Nanoparticles to Enable Background-Free *In Vivo* Photoacoustic Imaging. Nano Lett 2019, 19, 8109–8117. [PubMed: 31597418]

(19). Wang S; Fu L; Xin J; Wang S; Yao C; Zhang Z; Wang J Photoacoustic Response Induced by Nanoparticle-Mediated Photothermal Bubbles beyond the Thermal Expansion for Potential Theranostics. J. Biomed. Opt 2018, 23, 125002.

(20). Wilson K; Homan K; Emelianov S Biomedical Photoacoustics beyond Thermal Expansion Using Triggered Nanodroplet Vaporization for Contrast-Enhanced Imaging. Nat. Commun 2012, 3, 618. [PubMed: 22233628]

(21). Wang LV; Hu S Photoacoustic Tomography: *In Vivo* Imaging from Organelles to Organs. Science 2012, 335, 1458–1462. [PubMed: 22442475]

(22). Hashimoto S; Werner D; Uwada T Studies on the Interaction of Pulsed Lasers with Plasmonic Gold Nanoparticles toward Light Manipulation, Heat Management, and Nanofabrication. J. Photochem. Photobiol., C 2012, 13, 28–54.

(23). Dreaden EC; Alkilany AM; Huang X; Murphy CJ; El-Sayed MA The Golden Age: Gold Nanoparticles for Biomedicine. Chem. Soc. Rev 2012, 41, 2740–2779. [PubMed: 22109657]

(24). Alkilany AM; Murphy CJ Toxicity and Cellular Uptake of Gold Nanoparticles: What We Have Learned So Far? J. Nanopart. Res 2010, 12, 2313–2333. [PubMed: 21170131]

(25). Alkilany AM; Abulateefeh SR; Murphy CJ Facile Functionalization of Gold Nanoparticles with Plga Polymer Brushes and Efficient Encapsulation into Plga Nanoparticles: Toward Spatially Precise Bioimaging of Polymeric Nanoparticles. Part. Part. Syst. Charact 2018, 36, 1800414.

(26). Sun X; Liu Z; Welsher K; Robinson JT; Goodwin A; Zaric S; Dai H Nano-Graphene Oxide for Cellular Imaging and Drug Delivery. Nano Res 2008, 1, 203–212. [PubMed: 20216934]

(27). Irvine WM; Pollack JB Infrared Optical Properties of Water and Ice Spheres. Icarus 1968, 8, 324–360.

(28). Vogt WC; Jia C; Wear KA; Garra BS; Pfefer TJ Biologically Relevant Photoacoustic Imaging Phantoms with Tunable Optical and Acoustic Properties. J. Biomed. Opt 2016, 21, 101405. [PubMed: 26886681]

(29). Evanoff DD; Chumanov G Size-Controlled Synthesis of Nanoparticles. 2. Measurement of Extinction, Scattering, and Absorption Cross Sections. J. Phys. Chem. B 2004, 108, 13957–13962.

(30). Pang GA; Laufer J; Niessner R; Haisch C Photoacoustic Signal Generation in Gold Nanospheres in Aqueous Solution: Signal Generation Enhancement and Particle Diameter Effects. J. Phys. Chem. C 2016, 120, 27646–27656.

(31). Park J; Kang H; Kim YH; Lee S-W; Lee TG; Wi J-S Physically-Synthesized Gold Nanoparticles Containing Multiple Nanopores for Enhanced Photothermal Conversion and Photoacoustic Imaging. Nanoscale 2016, 8, 15514–15520. [PubMed: 27527067]

(32). Khan D; Gajula D; Bayram F; Kim S; Koley G Effect of Plasmonic Absorption on Photoacoustic Signal Generation. 2018 IEEE 13th Nanotechnology Materials and Devices Conference (NMDC) 2018, 1–4.

(33). Tao C; An L; Lin J; Tian Q; Yang S Surface Plasmon Resonance–Enhanced Photoacoustic Imaging and Photothermal Therapy of Endogenous H2s-Triggered Au@ Cu2o. Small 2019, 15, 1903473.

(34). Xu W; Leskinen J; Tick J; Happonen E; Tarvainen T; Lehto V-P Black Mesoporous Silicon as Contrast Agent for Led-Based 3D Photoacoustic Tomography. ACS Appl. Mater. Interfaces 2020, 12, 5456. [PubMed: 31920072]

(35). Lemaster J Gold Nanorods with Size-Controlled Polydopamine Coating for Spectral Imaging (Conference Presentation). Reporters, Markers, Dyes, Nanoparticles, and Molecular Probes for Biomedical Applications XII 2020, 112560A.

(36). Zhou J; Jiang Y; Hou S; Upputuri PK; Wu D; Li J; Wang P; Zhen X; Pramanik M; Pu K; et al. Compact Plasmonic Blackbody for Cancer Theranosis in the Near-Infrared II Window. ACS Nano 2018, 12, 2643–2651. [PubMed: 29438610]

(37). Repenko T; Rix A; Nedilko A; Rose J; Hermann A; Vinokur R; Moli S; Cao-Milàn R; Mayer M; von Plessen G; et al. Strong Photoacoustic Signal Enhancement by Coating Gold Nanoparticles with Melanin for Biomedical Imaging. Adv. Funct. Mater 2018, 28, 1705607.

(38). He L; Mao C; Brasino M; Harguindey A; Park W; Goodwin AP; Cha JN Tio2-Capped Gold Nanorods for Plasmon-Enhanced Production of Reactive Oxygen Species and Photothermal Delivery of Chemotherapeutic Agents. ACS Appl. Mater. Interfaces 2018, 10, 27965–27971. [PubMed: 30044085]

(39). Sreejith S; Joseph J; Nguyen KT; Murukeshan VM; Lye SW; Zhao Y Graphene Oxide Wrapping of Gold–Silica Core–Shell Nanohybrids for Photoacoustic Signal Generation and Bimodal Imaging. ChemNanoMat 2015, 1, 39–45.

(40). Moon H; Kumar D; Kim H; Sim C; Chang J-H; Kim J-M; Kim H; Lim D-K Amplified Photoacoustic Performance and Enhanced Photothermal Stability of Reduced Graphene Oxide Coated Gold Nanorods for Sensitive Photoacoustic Imaging. ACS Nano 2015, 9, 2711–2719. [PubMed: 25751167]

(41). Song J; Yang X; Jacobson O; Lin L; Huang P; Niu G; Ma Q; Chen X Sequential Drug Release and Enhanced Photothermal and Photoacoustic Effect of Hybrid Reduced Graphene Oxide-

Loaded Ultrasmall Gold Nanorod Vesicles for Cancer Therapy. ACS Nano 2015, 9, 9199–9209. [PubMed: 26308265]

(42). Leng C; Zhang X; Xu F; Yuan Y; Pei H; Sun Z; Li L; Bao Z Engineering Gold Nanorod–Copper Sulfide Heterostructures with Enhanced Photothermal Conversion Efficiency and Photostability. Small 2018, 14, 1703077.

(43). Yamaoka Y; Takamatsu T Enhancement of Multiphoton Excitation-Induced Photoacoustic Signals by Using Gold Nanoparticles Surrounded by Fluorescent Dyes. Proc. SPIE 2009, 71772A.

(44). Ferrauto G; Carniato F; Di Gregorio E; Tei L; Botta M; Aime S Large Photoacoustic Effect Enhancement for Icg Confined inside Mcm-41 Mesoporous Silica Nanoparticles. Nanoscale 2017, 9, 99–103. [PubMed: 27934996]

(45). Gao C; Deng Z-J; Peng D; Jin Y-S; Ma Y; Li Y-Y; Zhu Y-K; Xi J-Z; Tian J; Dai Z-F Near-Infrared Dye-Loaded Magnetic Nanoparticles as Photoacoustic Contrast Agent for Enhanced Tumor Imaging. Cancer Biol. Med 2016, 13, 349. [PubMed: 27807502]

(46). Novoselova MV; Bratashov DN; Sarimollaoglu M; Nedosekin DA; Harrington W; Watts A; Han M; Khlebtsov BN; Galanzha EI; Gorin DA; et al. Photoacoustic and Fluorescent Effects in Multilayer Plasmon-Dye Interfaces. J. Biophotonics 2019, 12, No. e201800265. [PubMed: 30511464]

(47). de la Zerda A; Bodapati S; Teed R; May SY; Tabakman SM; Liu Z; Khuri-Yakub BT; Chen X; Dai H; Gambhir SS Family of Enhanced Photoacoustic Imaging Agents for High-Sensitivity and Multiplexing Studies in Living Mice. ACS Nano 2012, 6, 4694–4701. [PubMed: 22607191]

(48). Zerda A. d. l.; Liu Z; Bodapati S; Teed R; Vaithilingam S; Khuri-Yakub BT; Chen X; Dai H; Gambhir SS Ultrahigh Sensitivity Carbon Nanotube Agents for Photoacoustic Molecular Imaging in Living Mice. Nano Lett 2010, 10, 2168–2172. [PubMed: 20499887]

(49). Liu Y; Bhattarai P; Dai Z; Chen X Photothermal Therapy and Photoacoustic Imaging *via* Nanotheranostics in Fighting Cancer. Chem. Soc. Rev 2019, 48, 2053–2108. [PubMed: 30259015]

(50). Halas NJ; Lal S; Chang W-S; Link S; Nordlander P Plasmons in Strongly Coupled Metallic Nanostructures. Chem. Rev 2011, 111, 3913–3961. [PubMed: 21542636]

(51). Jain PK; El-Sayed MA Plasmonic Coupling in Noble Metal Nanostructures. Chem. Phys. Lett 2010, 487, 153–164.

(52). Hohenester U Particle Plasmons. Nano and Quantum Optics 2020, 207–257.

(53). Tsai C-Y; Lin J-W; Wu C-Y; Lin P-T; Lu T-W; Lee P-T Plasmonic Coupling in Gold Nanoring Dimers: Observation of Coupled Bonding Mode. Nano Lett 2012, 12, 1648–1654. [PubMed: 22321005]

(54). Rasskazov IL; Wang L; Murphy CJ; Bhargava R; Carney PS Plasmon-Enhanced Upconversion: Engineering Enhancement and Quenching at Nano and Macro Scales. Opt. Mater. Express 2018, 8, 3787–3804.

(55). He L; Dragavon J; Cho S; Mao C; Yildirim A; Ma K; Chattaraj R; Goodwin AP; Park W; Cha JN Self-Assembled Gold Nanostar–Nayf 4: Yb/Er Clusters for Multimodal Imaging, Photothermal and Photodynamic Therapy. J. Mater. Chem. B 2016, 4, 4455–4461. [PubMed: 32263428]

(56). Funston AM; Novo C; Davis TJ; Mulvaney P Plasmon Coupling of Gold Nanorods at Short Distances and in Different Geometries. Nano Lett 2009, 9, 1651–1658. [PubMed: 19271775]

(57). Bohren CF; Huffman DR Absorption and Scattering of Light by Small Particles, revised ed.; John Wiley & Sons, 2008; 397–406.

(58). Chen T; Pourmand M; Feizpour A; Cushman B; Reinhard B. r. M. Tailoring Plasmon Coupling in Self-Assembled One-Dimensional Au Nanoparticle Chains through Simultaneous Control of Size and Gap Separation. J. Phys. Chem. Lett 2013, 4, 2147–2152. [PubMed: 24027605]

(59). Liu Y; He J; Yang K; Yi C; Liu Y; Nie L; Khashab NM; Chen X; Nie Z Folding up of Gold Nanoparticle Strings into Plasmonic Vesicles for Enhanced Photoacoustic Imaging. Angew. Chem., Int. Ed 2015, 54, 15809–15812.

(60). Huang P; Lin J; Li W; Rong P; Wang Z; Wang S; Wang X; Sun X; Aronova M; Niu G; et al. Biodegradable Gold Nanovesicles with an Ultrastrong Plasmonic Coupling Effect for

Photoacoustic Imaging and Photothermal Therapy. Angew. Chem., Int. Ed 2013, 52, 13958–13964.

(61). Yang Z; Song J; Dai Y; Chen J; Wang F; Lin L; Liu Y; Zhang F; Yu G; Zhou Z; et al. Self-Assembly of Semiconducting-Plasmonic Gold Nanoparticles with Enhanced Optical Property for Photoacoustic Imaging and Photothermal Therapy. Theranostics 2017, 7, 2177. [PubMed: 28740543]

(62). Park JH; Dumani DS; Arsiwala A; Emelianov S; Kane RS Tunable Aggregation of Gold-Silica Janus Nanoparticles to Enable Contrast-Enhanced Multiwavelength Photoacoustic Imaging *In Vivo*. Nanoscale 2018, 10, 15365–15370. [PubMed: 30083665]

(63). Lu SZ; Guo XY; Zou MS; Zheng ZQ; Li YC; Li XD; Li LL; Wang H Bacteria-Instructed *In Situ* Aggregation of Aunps with Enhanced Photoacoustic Signal for Bacterial Infection Bioimaging. Adv. Healthcare Mater 2020, 9, 1901229.

(64). Murphy CJ; Sau TK; Gole AM; Orendorff CJ; Gao J; Gou L; Hunyadi SE; Li T Anisotropic Metal Nanoparticles: Synthesis, Assembly, and Optical Applications. J. Phys. Chem. B 2005, 109, 13857–13870. [PubMed: 16852739]

(65). Li W; Chen X Gold Nanoparticles for Photoacoustic Imaging. Nanomedicine 2015, 10, 299–320. [PubMed: 25600972]

(66). Jokerst JV; Miao Z; Zavaleta C; Cheng Z; Gambhir SS Affibody-Functionalized Gold–Silica Nanoparticles for Raman Molecular Imaging of the Epidermal Growth Factor Receptor. Small 2011, 7, 625–633. [PubMed: 21302357]

(67). Wu X; Ming T; Wang X; Wang P; Wang J; Chen J High-Photoluminescence-Yield Gold Nanocubes: For Cell Imaging and Photothermal Therapy. ACS Nano 2010, 4, 113–120. [PubMed: 20014823]

(68). Peng Y; Liu Y; Lu X; Wang S; Chen M; Huang W; Wu Z; Lu G; Nie L Ag-Hybridized Plasmonic Au-Triangular Nanoplates: Highly Sensitive Photoacoustic/Raman Evaluation and Improved Antibacterial/Photothermal Combination Therapy. J. Mater. Chem. B 2018, 6, 2813–2820. [PubMed: 32254234]

(69). Mantri Y; Jokerst JV Ferricyanide Meditated Photoacoustic Enhancement of Metal Chalcogenide-Coated Gold Nanorods. (Conference Presentation). Photons Plus Ultrasound: Imaging and Sensing 2020 2020, 1124019.

(70). Kim T; Zhang Q; Li J; Zhang L; Jokerst JV A Gold/Silver Hybrid Nanoparticle for Treatment and Photoacoustic Imaging of Bacterial Infection. ACS Nano 2018, 12, 5615–5625. [PubMed: 29746090]

(71). Jana NR; Gearheart L; Murphy CJ Wet Chemical Synthesis of High Aspect Ratio Cylindrical Gold Nanorods. J. Phys. Chem. B 2001, 105, 4065–4067.

(72). Moon GD; Choi S-W; Cai X; Li W; Cho EC; Jeong U; Wang LV; Xia Y A New Theranostic System Based on Gold Nanocages and Phase-Change Materials with Unique Features for Photoacoustic Imaging and Controlled Release. J. Am. Chem. Soc 2011, 133, 4762–4765. [PubMed: 21401092]

(73). Li W; Brown PK; Wang LV; Xia Y Gold Nanocages as Contrast Agents for Photoacoustic Imaging. Contrast Media Mol. Imaging 2011, 6, 370–377. [PubMed: 22025337]

(74). Yang X; Skrabalak SE; Li Z-Y; Xia Y; Wang LV Photoacoustic Tomography of a Rat Cerebral Cortex *In Vivo* with Au Nanocages as an Optical Contrast Agent. Nano Lett 2007, 7, 3798–3802. [PubMed: 18020475]

(75). Xiang L; Xing D; Gu H; Yang D; Zeng L; Yang S Gold Nanoshell-Based Photoacoustic Imaging Application in Biomedicine. International Symposium on Biophotonics, Nanophotonics and Meta-materials 2006, 76–79.

(76). Liu M; Guyot-Sionnest P Preparation and Optical Properties of Silver Chalcogenide Coated Gold Nanorods. J. Mater. Chem 2006, 16, 3942–3945.

(77). Chen H; Kou X; Yang Z; Ni W; Wang J Shape-and Size-Dependent Refractive Index Sensitivity of Gold Nanoparticles. Langmuir 2008, 24, 5233–5237. [PubMed: 18435552]

(78). Zhang X-L; Zheng C; Zhang Y; Yang H-H; Liu X; Liu J One-Pot Synthesis of Gold Nanostars Using Plant Polyphenols for Cancer Photoacoustic Imaging and Photothermal Therapy. J. Nanopart. Res 2016, 18, 174.

(79). Grześkiewicz B; Ptaszyński K; Kotkowiak M Near and Far-Field Properties of Nanoprisms with Rounded Edges. Plasmonics 2014, 9, 607–614. [PubMed: 24834020]

(80). Huang W; Qian W; El-Sayed MA; Ding Y; Wang ZL Effect of the Lattice Crystallinity on the Electron–Phonon Relaxation Rates in Gold Nanoparticles. J. Phys. Chem. C 2007, 111, 10751–10757.

(81). Link S; Burda C; Mohamed M; Nikoobakht B; El-Sayed M Femtosecond Transient-Absorption Dynamics of Colloidal Gold Nanorods: Shape Independence of the Electron-Phonon Relaxation Time. Phys. Rev. B: Condens. Matter Mater. Phys 2000, 61, 6086.

(82). Liu JG; Zhang H; Link S; Nordlander P Relaxation of Plasmon-Induced Hot Carriers. ACS Photonics 2018, 5, 2584–2595.

(83). He W; Wang X; Gao X; Lu Z; Song J Application of Gold Nanoparticles in Photoacoustic Imaging. IOP Conf. Ser.: Mater. Sci. Eng 2020, 729, 012086.

(84). García-Álvarez R; Chen L; Nedilko A; Sánchez-Iglesias A; Rix A; Lederle W; Pathak V; Lammers T; von Plessen G; Kostarelos K; et al. Optimizing the Geometry of Photoacoustically Active Gold Nanoparticles for Biomedical Imaging. ACS Photonics 2020, 7, 646–652.

(85). Knights OB; Ye S; Ingram N; Freear S; McLaughlan JR Optimising Gold Nanorods for Photoacoustic Imaging *In Vitro*. Nanoscale Adv 2019, 1, 1472–1481.

(86). Jiang Y; Upputuri PK; Xie C; Lyu Y; Zhang L; Xiong Q; Pramanik M; Pu K Broadband Absorbing Semiconducting Polymer Nanoparticles for Photoacoustic Imaging in Second Near-Infrared Window. Nano Lett 2017, 17, 4964–4969. [PubMed: 28654292]

(87). Cao Z; Feng L; Zhang G; Wang J; Shen S; Li D; Yang X Semiconducting Polymer-Based Nanoparticles with Strong Absorbance in NIR-II Window for *In Vivo* Photothermal Therapy and Photoacoustic Imaging. Biomaterials 2018, 155, 103–111. [PubMed: 29175079]

(88). Wu J; You L; Lan L; Lee HJ; Chaudhry ST; Li R; Cheng JX; Mei J Semiconducting Polymer Nanoparticles for Centimeters-Deep Photoacoustic Imaging in the Second Near-Infrared Window. Adv. Mater 2017, 29, 1703403.

(89). Chen Y-S; Zhao Y; Yoon SJ; Gambhir SS; Emelianov S Miniature Gold Nanorods for Photoacoustic Molecular Imaging in the Second Near-Infrared Optical Window. Nat. Nanotechnol 2019, 14, 465–472. [PubMed: 30833692]

(90). Oldenburg S; Averitt R; Westcott S; Halas N Nano-engineering of Optical Resonances. Chem. Phys. Lett 1998, 288, 243–247.

(91). Wang S; Xu H; Ye J Plasmonic Rod-in-Shell Nanoparticles for Photothermal Therapy. Phys. Chem. Chem. Phys 2014, 16, 12275–12281. [PubMed: 24818860]

(92). Vijayaraghavan P; Chiang CS; Chiang HK; Li ML; Hwang KC Multi-Branched Plasmonic Gold Nanoechinus-Based Triple Modal Bioimaging: An Efficient Nir-to-Nir up and Down-Conversion Emission and Photoacoustic Imaging. Adv. Mater. Technol. (Weinheim, Ger.) 2016, 1, 1600107.

(93). Ge X; Fu Q; Bai L; Chen B; Wang R; Gao S; Song J Photoacoustic Imaging and Photothermal Therapy in the Second Near-Infrared Window. New J. Chem 2019, 43, 8835–8851.

(94). Chen YS; Frey W; Aglyamov S; Emelianov S Environment-Dependent Generation of Photoacoustic Waves from Plasmonic Nanoparticles. Small 2012, 8, 47–52. [PubMed: 22114029]

(95). Shi Y; Qin H; Yang S; Xing D Thermally Confined Shell Coating Amplifies the Photoacoustic Conversion Efficiency of Nanoprobes. Nano Res 2016, 9, 3644–3655.

(96). Shahbazi K; Frey W; Chen Y-S; Aglyamov S; Emelianov S Photoacoustics of Core–Shell Nanospheres Using Comprehensive Modeling and Analytical Solution Approach. Commun. Phys 2019, 2, 119.

(97). Jokerst JV; Thangaraj M; Kempen PJ; Sinclair R; Gambhir SS Photoacoustic Imaging of Mesenchymal Stem Cells in Living Mice *via* Silica-Coated Gold Nanorods. ACS Nano 2012, 6, 5920–5930. [PubMed: 22681633]

(98). Chen Y-S; Frey W; Kim S; Kruizinga P; Homan K; Emelianov S Silica-Coated Gold Nanorods as Photoacoustic Signal Nanoamplifiers. Nano Lett 2011, 11, 348–354. [PubMed: 21244082]

(99). Chen Y-S; Frey W; Kim S; Homan K; Kruizinga P; Sokolov K; Emelianov S Enhanced Thermal Stability of Silica-Coated Gold Nanorods for Photoacoustic Imaging and Image-Guided Therapy. Opt. Express 2010, 18, 8867–8878. [PubMed: 20588732]

(100). Gao F; Bai L; Liu S; Zhang R; Zhang J; Feng X; Zheng Y; Zhao Y Rationally Encapsulated Gold Nanorods Improving Both Linear and Nonlinear Photoacoustic Imaging Contrast *In Vivo*. Nanoscale 2017, 9, 79–86. [PubMed: 27911452]

(101). Ju K-Y; Kang J; Pyo J; Lim J; Chang JH; Lee J-K Ph-Induced Aggregated Melanin Nanoparticles for Photoacoustic Signal Amplification. Nanoscale 2016, 8, 14448–14456. [PubMed: 27406260]

(102). Bayer CL; Nam SY; Chen Y-S; Emelianov SY Photoacoustic Signal Amplification through Plasmonic Nanoparticle Aggregation. J. Biomed. Opt 2013, 18, No. 016001.

(103). Chen Y-S; Yoon SJ; Frey W; Dockery M; Emelianov S Dynamic Contrast-Enhanced Photoacoustic Imaging Using Photothermal Stimuli-Responsive Composite Nanomodulators. Nat. Commun 2017, 8, 15782. [PubMed: 28593942]

(104). Alkurdi A; Lombard J; Detcheverry F; Merabia S Enhanced Heat Transfer with Metal-Dielectric Core-Shell Nanoparticles. Phys. Rev. Appl 2020, 13, No. 034036.

(105). Kumar D; Ghai DP; Soni R Simulation Studies of Photoacoustic Response from Gold-Silica Core-Shell Nanoparticles. Plasmonics 2018, 13, 1833–1841.

(106). Pang GA; Poisson F; Laufer J; Haisch C; Bossy E Theoretical and Experimental Study of Photoacoustic Excitation of Silica-Coated Gold Nanospheres in Water. J. Phys. Chem. C 2020, 124, 1088–1098.

(107). Hu M; Wang X; Hartland GV; Salgueiriño-Maceira V; Liz-Marzán LM Heat Dissipation in Gold–Silica Core-Shell Nanoparticles. Chem. Phys. Lett 2003, 372, 767–772.

(108). Rodríguez-Roldán G; Cruz-Orea A; Suaste-Gómez E Thermal Characterization of a Ppy/Pla Composite by Photoacoustic Calorimetry and Photopyroelectric Techniques. Int. J. Thermophys 2019, 40, 16.

(109). Hatef A; Darvish B; Dagallier A; Davletshin YR; Johnston W; Kumaradas JC; Rioux D; Meunier M Analysis of Photoacoustic Response from Gold–Silver Alloy Nanoparticles Irradiated by Short Pulsed Laser in Water. J. Phys. Chem. C 2015, 119, 24075–24080.

(110). Nam SY; Ricles LM; Suggs LJ; Emelianov SY Nonlinear Photoacoustic Signal Increase from Endocytosis of Gold Nanoparticles. Opt. Lett 2012, 37, 4708–4710. [PubMed: 23164887]

(111). Masim FCP; Liu H-L; Porta M; Yonezawa T; Balčytis A; Juodkazis S; Hsu W-H; Hatanaka K Enhanced Photoacoustics from Gold Nano-Colloidal Suspensions under Femtosecond Laser Excitation. Opt. Express 2016, 24, 14781–14792. [PubMed: 27410630]

(112). Langer G; Bouchal K-D; Grün H; Burgholzer P; Berer T Two-Photon Absorption-Induced Photoacoustic Imaging of Rhodamine B Dyed Polyethylene Spheres Using a Femtosecond Laser. Opt. Express 2013, 21, 22410–22422. [PubMed: 24104130]

(113). Masim FCP; Hsu W-H; Liu H-L; Yonezawa T; Balčytis A; Juodkazis S; Hatanaka K Photoacoustic Signal Enhancements from Gold Nano-Colloidal Suspensions Excited by a Pair of Time-Delayed Femtosecond Pulses. Opt. Express 2017, 25, 19497–19507. [PubMed: 29041143]

(114). Huang K; Zhang Y; Lin J; Huang P Nanomaterials for Photoacoustic Imaging in the Second Near-Infrared Window. Biomater. Sci 2019, 7, 472–479. [PubMed: 30255873]

(115). Petronijevic E; Leahu G; Belardini A; Centini M; Li Voti R; Hakkarainen T; Koivusalo E; Rizzo Piton M; Suomalainen S; Guina M; et al. Photo-Acoustic Spectroscopy Reveals Extrinsic Optical Chirality in Gaas-Based Nanowires Partially Covered with Gold. Int. J. Thermophys 2018, 39, 46.

(116). Jeong H-H; Mark AG; Alarcón-Correa M; Kim I; Oswald P; Lee T-C; Fischer P Dispersion and Shape Engineered Plasmonic Nanosensors. Nat. Commun 2016, 7, 11331. [PubMed: 27090866]

(117). Petronijević E; Leahu G; Li Voti R; Belardini A; Scian C; Michieli N; Cesca T; Mattei G; Sibilia C Photo-Acoustic Detection of Chirality in Metal-Polystyrene Metasurfaces. Appl. Phys. Lett 2019, 114, No. 053101.

(118). Nishi H; Asami K; Tatsuma T Cus Nanoplates for Lspr Sensing in the Second Biological Optical Window. Opt. Mater. Express 2016, 6, 1043–1048.

(119). Lei DY; Appavoo K; Ligmajer F; Sonnefraud Y; Haglund RF Jr; Maier SA Optically-Triggered Nanoscale Memory Effect in a Hybrid Plasmonic-Phase Changing Nanostructure. ACS Photonics 2015, 2, 1306–1313.

(120). Yildirim A; Chattaraj R; Blum NT; Goodwin AP Understanding Acoustic Cavitation Initiation by Porous Nanoparticles: Toward Nanoscale Agents for Ultrasound Imaging and Therapy. Chem. Mater 2016, 28, 5962–5972. [PubMed: 28484307]

(121). Hariri A; Alipour K; Mantri Y; Schulze JP; Jokerst JV Deep Learning Improves Contrast in Low-Fluence Photoacoustic Imaging. Biomed. Opt. Express 2020, 11, 3360–3373. [PubMed: 32637260]

(122). Phan TTV; Bui NQ; Moorthy MS; Lee KD; Oh J Synthesis and *In Vitro* Performance of Polypyrrole-Coated Iron–Platinum Nanoparticles for Photothermal Therapy and Photoacoustic Imaging. Nanoscale Res. Lett 2017, 12, 570. [PubMed: 29046993]

(123). Lee DY; Kim JY; Lee Y; Lee S; Miao W; Kim HS; Min JJ; Jon S Black Pigment Gallstone Inspired Platinum-Chelated Bilirubin Nanoparticles for Combined Photoacoustic Imaging and Photothermal Therapy of Cancers. Angew. Chem 2017, 129, 13872–13876.

(124). Homan KA; Souza M; Truby R; Luke GP; Green C; Vreeland E; Emelianov S Silver Nanoplate Contrast Agents for *In Vivo* Molecular Photoacoustic Imaging. ACS Nano 2012, 6, 641–650. [PubMed: 22188516]

(125). Silvestri B; Armanetti P; Sanità G; Vitiello G; Lamberti A; Calì G; Pezzella A; Luciani G; Menichetti L; Luin S; et al. Silver-Nanoparticles as Plasmon-Resonant Enhancers for Eumelanin's Photoacoustic Signal in a Self-Structured Hybrid Nanoprobe. Mater. Sci. Eng., C 2019, 102, 788–797.

(126). Ku G; Zhou M; Song S; Huang Q; Hazle J; Li C Copper Sulfide Nanoparticles as a New Class of Photoacoustic Contrast Agent for Deep Tissue Imaging at 1064 Nm. ACS Nano 2012, 6, 7489–7496. [PubMed: 22812694]

(127). Song XR; Wang X; Yu SX; Cao J; Li SH; Li J; Liu G; Yang HH; Chen X Co9se8 Nanoplates as a New Theranostic Platform for Photoacoustic/Magnetic Resonance Dual-Modal-Imaging-Guided Chemo-Photothermal Combination Therapy. Adv. Mater 2015, 27, 3285–3291. [PubMed: 25885638]

(128). Cheng L; Liu J; Gu X; Gong H; Shi X; Liu T; Wang C; Wang X; Liu G; Xing H; et al. Pegylated Ws2 Nanosheets as a Multifunctional Theranostic Agent for *In Vivo* Dual-Modal Ct/Photoacoustic Imaging Guided Photothermal Therapy. Adv. Mater 2014, 26, 1886–1893. [PubMed: 24375758]

(129). Yu X; Li A; Zhao C; Yang K; Chen X; Li W Ultrasmall Semimetal Nanoparticles of Bismuth for Dual-Modal Computed Tomography/Photoacoustic Imaging and Synergistic Thermoradiotherapy. ACS Nano 2017, 11, 3990–4001. [PubMed: 28395135]

(130). Zhang YS; Wang Y; Wang L; Wang Y; Cai X; Zhang C; Wang LV; Xia Y Labeling Human Mesenchymal Stem Cells with Gold Nanocages for *In Vitro* and *In Vivo* Tracking by Two-Photon Microscopy and Photoacoustic Microscopy. Theranostics 2013, 3, 532. [PubMed: 23946820]

(131). Thakur SN; Guo D; Kundu T; Goodman L Two-Photon Photoacoustic Spectroscopy of Acetone 3p Rydberg States. Chem. Phys. Lett 1992, 199, 335–340.

(132). Nie L; Chen M; Sun X; Rong P; Zheng N; Chen X Palladium Nanosheets as Highly Stable and Effective Contrast Agents for *In Vivo* Photoacoustic Molecular Imaging. Nanoscale 2014, 6, 1271–1276. [PubMed: 24317132]

(133). Chen F; Zhao ER; Hableel G; Hu T; Kim T; Li J; Gonzalez-Pech NI; Cheng DJ; Lemaster JE; Xie Y; et al. Increasing the Efficacy of Stem Cell Therapy *via* Triple-Function Inorganic Nanoparticles. ACS Nano 2019, 13, 6605–6617. [PubMed: 31188564]

(134). Lemaster JE; Chen F; Kim T; Hariri A; Jokerst JV Development of a Trimodal Contrast Agent for Acoustic and Magnetic Particle Imaging of Stem Cells. ACS Appl. Nano Mater 2018, 1, 1321–1331.

(135). Reguera J; Jiménez de Aberasturi D; Henriksen-Lacey M; Langer J; Espinosa A; Szczupak B; Wilhelm C; Liz-Marzán LM Janus Plasmonic–Magnetic Gold–Iron Oxide Nanoparticles as Contrast Agents for Multimodal Imaging. Nanoscale 2017, 9, 9467–9480. [PubMed: 28660946]

(136). Kim J-W; Galanzha EI; Shashkov EV; Moon H-M; Zharov VP Golden Carbon Nanotubes as Multimodal Photoacoustic and Photothermal High-Contrast Molecular Agents. Nat. Nanotechnol 2009, 4, 688. [PubMed: 19809462]

(137). Nima ZA; Watanabe F; Jamshidi-Parsian A; Sarimollaoglu M; Nedosekin DA; Han M; Watts JA; Biris AS; Zharov VP; Galanzha EI Bioinspired Magnetic Nanoparticles as Multimodal Photoacoustic, Photothermal and Photomechanical Contrast Agents. Sci. Rep 2019, 9, 887. [PubMed: 30696936]

(138). Rieffel J; Chitgupi U; Lovell JF Recent Advances in Higher-Order, Multimodal, Biomedical Imaging Agents. Small 2015, 11, 4445–4461. [PubMed: 26185099]

(139). Chen P-J; Hu S-H; Fan C-T; Li M-L; Chen Y-Y; Chen S-Y; Liu D-M A Novel Multifunctional Nano-Platform with Enhanced Anti-Cancer and Photoacoustic Imaging Modalities Using Gold-Nanorod-Filled Silica Nanobeads. Chem. Commun. (Cambridge, U. K.) 2013, 49, 892–894.

(140). Chen D; Wang C; Nie X; Li S; Li R; Guan M; Liu Z; Chen C; Wang C; Shu C; et al. Photoacoustic Imaging Guided Near-Infrared Photothermal Therapy Using Highly Water-Dispersible Single-Walled Carbon Nanohorns as Theranostic Agents. Adv. Funct. Mater 2014, 24, 6621–6628.

(141). Riley RS; Day ES Gold Nanoparticle-Mediated Photothermal Therapy: Applications and Opportunities for Multimodal Cancer Treatment. Wiley Interdiscip. Rev.: Nanomed. Nanobiotechnol 2017, 9, No. e1449.

(142). Moore C; Chen F; Wang J; Jokerst JV Listening for the Therapeutic Window: Advances in Drug Delivery Utilizing Photoacoustic Imaging. Adv. Drug Delivery Rev 2019, 144, 78–89.

(143). Wang L; Jiang X; Ji Y; Bai R; Zhao Y; Wu X; Chen C Surface Chemistry of Gold Nanorods: Origin of Cell Membrane Damage and Cytotoxicity. Nanoscale 2013, 5, 8384–8391. [PubMed: 23873113]

(144). Alkilany AM; Nagaria PK; Hexel CR; Shaw TJ; Murphy CJ; Wyatt MD Cellular Uptake and Cytotoxicity of Gold Nanorods: Molecular Origin of Cytotoxicity and Surface Effects. Small 2009, 5, 701–708. [PubMed: 19226599]

(145). Jokerst JV; Lobovkina T; Zare RN; Gambhir SS Nanoparticle Pegylation for Imaging and Therapy. Nanomedicine 2011, 6, 715–728. [PubMed: 21718180]

(146). Takahashi H; Niidome Y; Niidome T; Kaneko K; Kawasaki H; Yamada S Modification of Gold Nanorods Using Phosphatidylcholine to Reduce Cytotoxicity. Langmuir 2006, 22, 2–5. [PubMed: 16378388]

(147). Yasun E; Li C; Barut I; Janvier D; Qiu L; Cui C; Tan W Bsa Modification to Reduce Ctab Induced Nonspecificity and Cytotoxicity of Aptamer-Conjugated Gold Nanorods. Nanoscale 2015, 7, 10240–10248. [PubMed: 25990591]

(148). Lee YJ; Ahn E-Y; Park Y Shape-Dependent Cytotoxicity and Cellular Uptake of Gold Nanoparticles Synthesized Using Green Tea Extract. Nanoscale Res. Lett 2019, 14, 129. [PubMed: 30976946]

(149). Rastinehad AR; Anastos H; Wajswol E; Winoker JS; Sfakianos JP; Doppalapudi SK; Carrick MR; Knauer CJ; Taouli B; Lewis SC; et al. Gold Nanoshell-Localized Photothermal Ablation of Prostate Tumors in a Clinical Pilot Device Study. Proc. Natl. Acad. Sci. U. S. A 2019, 116, 18590–18596. [PubMed: 31451630]

(150). Viator JA; Svaasand LO; Aguilar G; Choi B; Nelson JS Photoacoustic Measurement of Epidermal Melanin. Proc. SPIE 2003, 14–20.

(151). Zhang HF; Maslov K; Stoica G; Wang LV Functional Photoacoustic Microscopy for High-Resolution and Noninvasive *In Vivo* Imaging. Nat. Biotechnol 2006, 24, 848–851. [PubMed: 16823374]

(152). West JL; Halas NJ Engineered Nanomaterials for Biophotonics Applications: Improving Sensing, Imaging, and Therapeutics. Annu. Rev. Biomed. Eng 2003, 5, 285–292. [PubMed: 14527314]

(153). Lal S; Clare SE; Halas NJ Nanoshell-Enabled Photothermal Cancer Therapy: Impending Clinical Impact. Acc. Chem. Res 2008, 41, 1842–1851. [PubMed: 19053240]

VOCABULARY

Absorption coefficient, μ_a (cm^{-1}), describes how well a material absorbs incident photons at a defined wavelength; Thermal expansion coefficient, β (K^{-1}), describes how the size of an object changes as a function of temperature; Specific heat capacity, C_p (J/(K kg)), describes the amount of thermal energy required to raise the temperature of a substance per unit of mass; Fluence, *F*, describes the laser pulse energy (J) incident on the effective focal spot (cm^2); Localized surface plasmon resonance (LSPR), describes the locally confined resonant oscillation of conduction electrons upon light irradiation

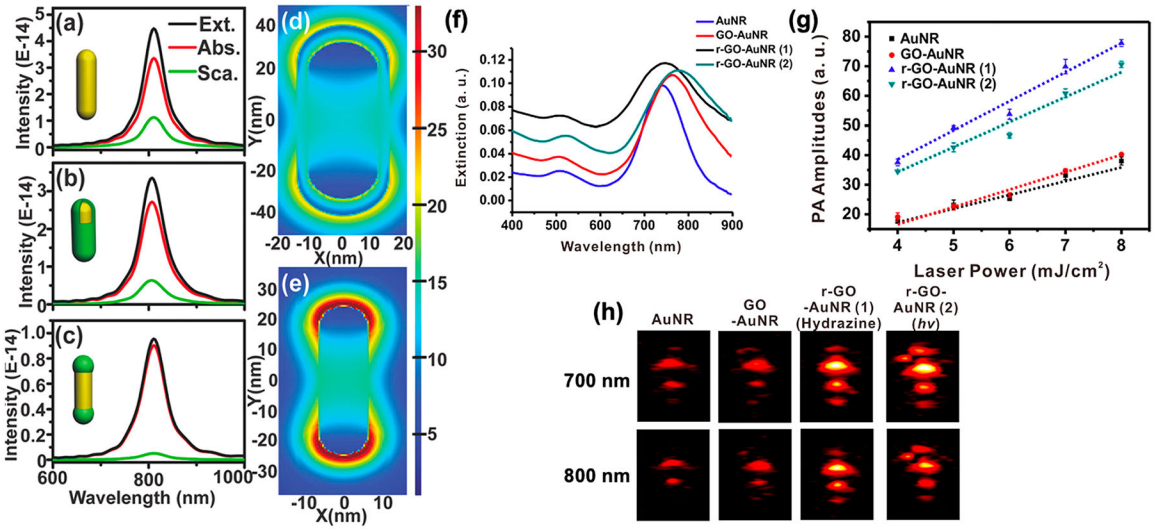

Figure 1.

Increasing absorbance enhances PA. (a–c) Calculated extinction (Ext.), absorption (Abs.), and scattering (Sca.) spectra of AuNRs, core–shell, and dumbbell-like AuNRs–Cu_7S_4 heterostructures, respectively. Adding Cu_7S_4 on the tips versus a shell increases absorption and reduces scattering. (d,e) FDTD simulations of the localized electric field of (d) core–shell and (e) dumbbell-like AuNRs–Cu_7S_4 heterostructures show electric-field enhancement when Cu_7S_4 is deposited on AuNR tips. (f) Wrapping with reduced graphene oxides increases the absorbance at 700 and 800 nm. (g) PA amplitude acquired with increasing laser power inputs for samples presented in (f). Wrapping with reduced graphene oxide enhances the PA signal by 2-fold compared to unwrapped controls. (h) PA images obtained at 700 and 800 nm (laser power: 6.2 mJ/cm^2; pulse rate: 10 Hz). Panels (a–e) were reprinted with permission from ref 42. Copyright 2018 John Wiley and Sons. Panels (f–h) were adapted with permission from ref 40. Copyright 2015 American Chemical Society.

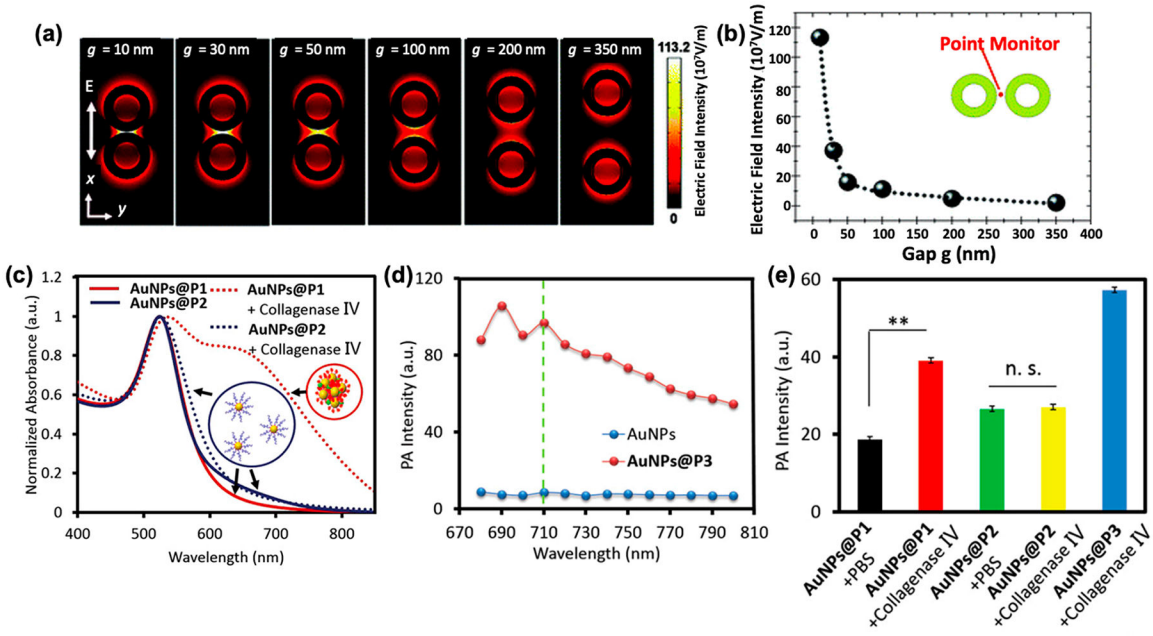

Figure 2.

Plasmonic coupling causing local-field enhancement and spectral shifts. (a) Electric-field intensity distribution on top surface and (b) within the interparticle gap as a function of distance (g) between two gold nanorings. As *g* reduces, the electric-field intensity between the two particles is enhanced due to plasmonic coupling. (c) Induced aggregation and plasmon coupling causes a red-shift in the absorption spectrum. As a result, the absorbance at 710 nm increases. (d,e) Aggregation-based enhancement of the PA signal *in vitro*. (d) PA intensity curves of AuNPs and AuNPs@P3—a positive control that self-aggregates showing that increased NIR absorbance leads to a higher PA signal compared to the unaggregated control. (e) PA signal of AuNPs@P1 and AuNPs@P2 (negative control) treated with collagenase IV for 3 h in PBS buffer. Nanoparticles aggregated in the presence of collagenase IV results in a higher PA signal. Panels (a,b) were reprinted with permission from ref 53. Copyright 2012 American Chemical Society. Panels (c–e) were reprinted with permission from ref 63. Copyright 2020 John Wiley and Sons.

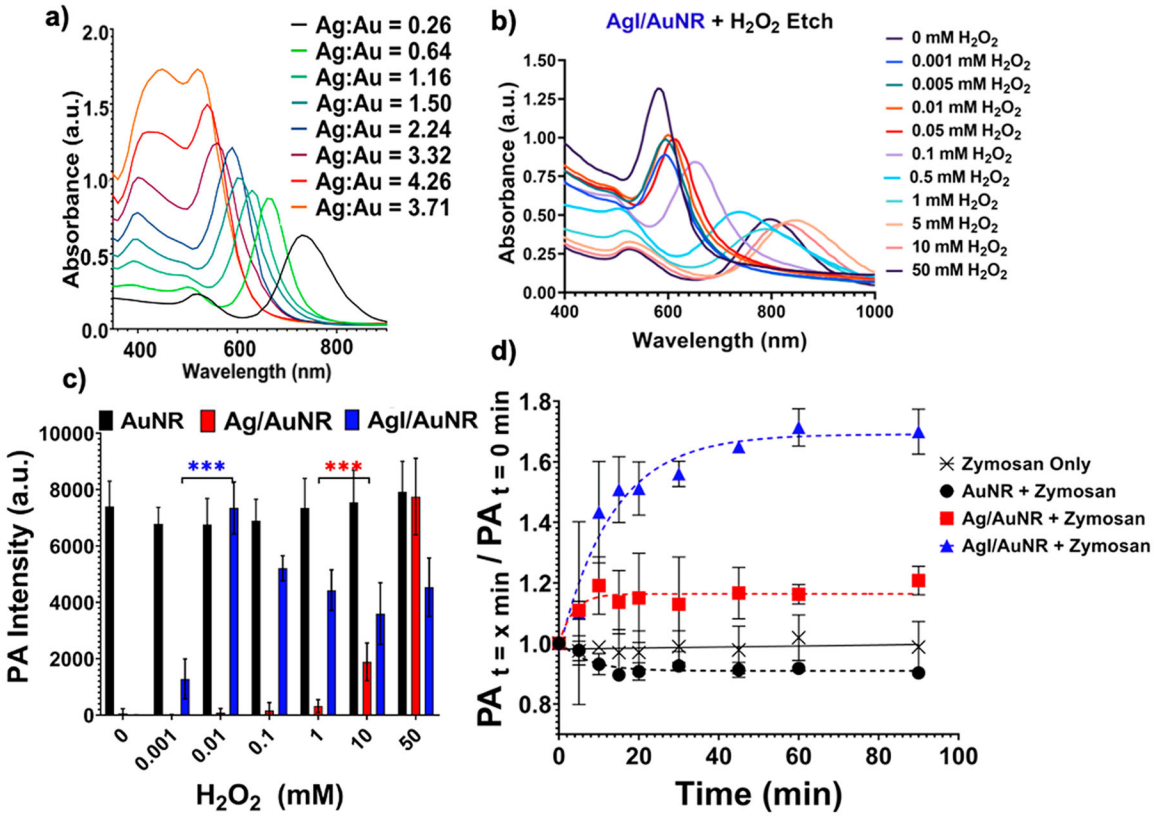

Figure 3.

Spectral shifts affect the absorption coefficient. (a) Absorption spectra of silver-coated AuNRs with increasing shell thickness (right to left). Increasing shell thickness causes a blue-shift in the absorption spectra due to a reduction in the AuNR aspect ratio. The μ_a at 680 nm reduces because of the blue-shift. (b) Selective etching of the silver shell with an increasing concentration of reactive oxygen species (H_2O_2) restores the AuNR absorption and μ_a at 680 nm. (c) PA intensity at 680 nm increases as a function of H_2O_2 concentration as μ_a increases in (b). (d) *In vivo* detection of oxidative stress as a function of time. Iodide-doped silver-coated particles are more sensitive to oxidative stress and show a 70% increase in PA intensity over 90 min (680 nm). Adapted with permission from ref 13. Copyright 2020 The Royal Society of Chemistry.

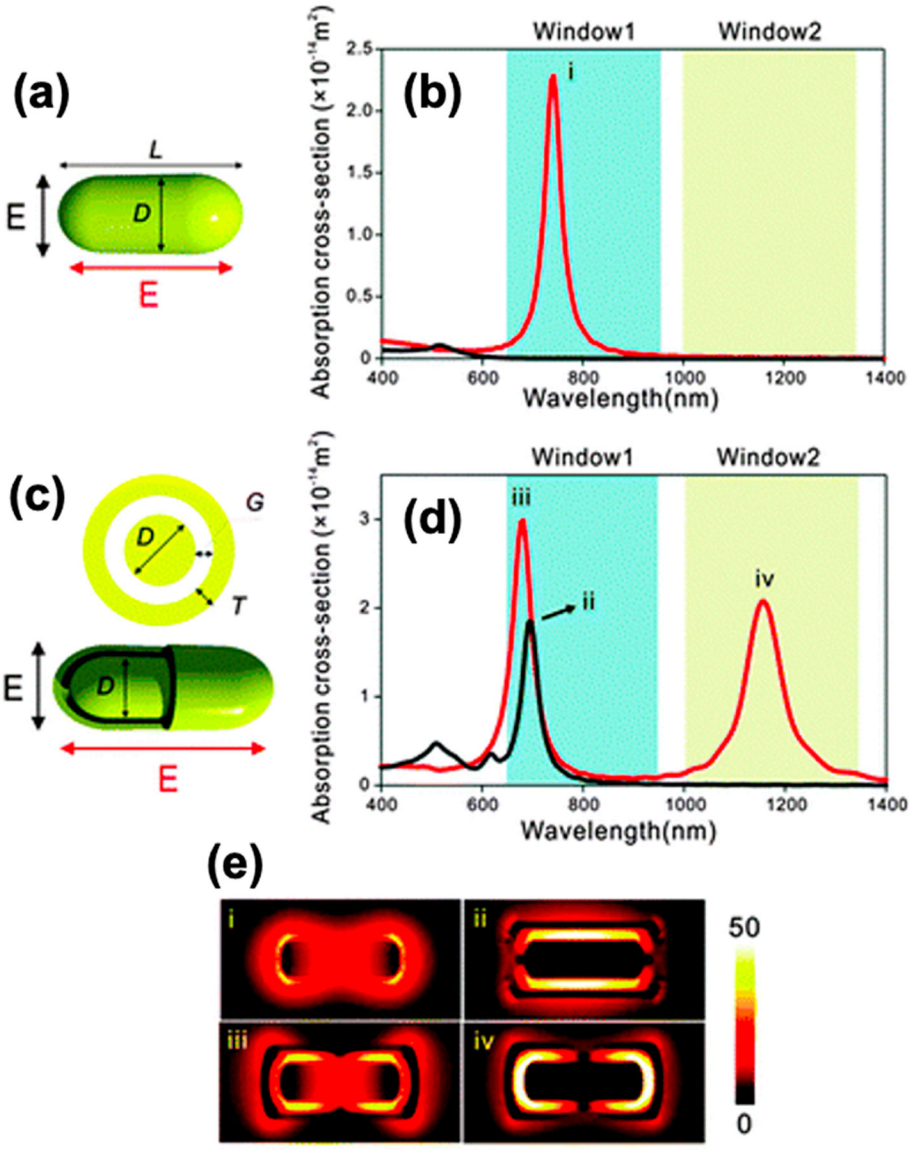

Figure 4.

Moving plasmonics into the NIR-II window. (a,c) Schematic illustrations and (b,d) calculated absorption spectra of (a,d) a Au nanorod (D = 20 nm, L = 60 nm) or (c,d) a Au rod-in-shell particle (D = 20 nm, L = 60 nm, T = 4 nm, and G = 5 nm) when illuminated by the (black) transversely or (red) longitudinally polarized light. The blue and yellow shaded areas indicate the NIR-I and -II biological optical windows, respectively. (e) Near-field intensity distribution of the resonance modes (i–iv). Reprinted with permission from ref 91. Copyright 2014 The Royal Society of Chemistry.

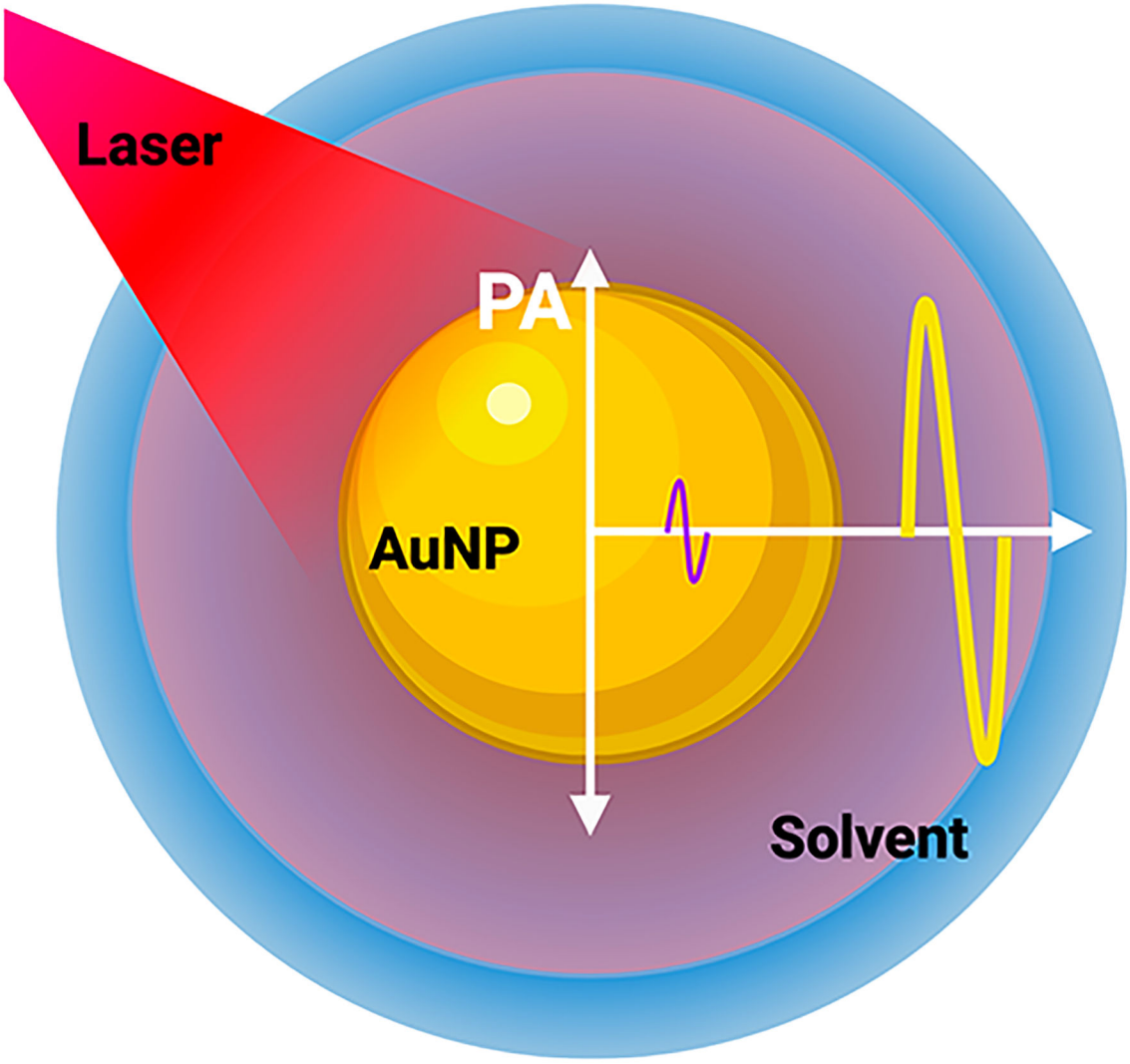

Figure 5.

Solvent-generated PA signal. During a laser pulse, heat is transferred into the solvent, which undergoes thermoelastic expansion and produces up to 93% of the PA response (yellow curve) compared to the absorbing nanoparticle (purple curve). PA amplitude is directly proportional to the rate of heat flux from the nanoparticle to the solvent and depends on the laser pulse width, Kapitza resistance (thermal resistance at the nanoparticle–solvent interface), and the thermoelastic properties of the solvent itself. The red region around the nanoparticle depicts the heated region of the solvent.

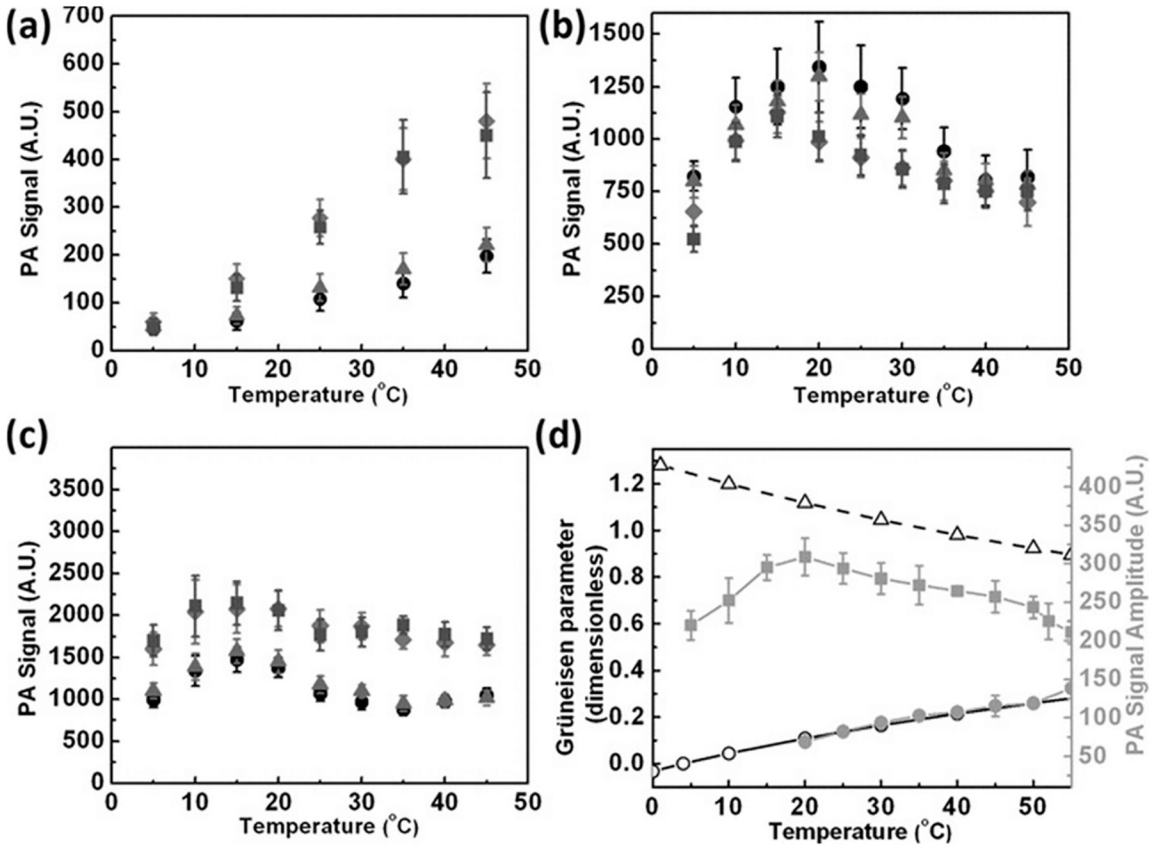

Figure 6.

PA is proportional to the thermal expansion coefficient of the solvent. Thermal expansion coefficient and the Grüneisen parameter are directly proportional to each other. The PA amplitude of gold nanospheres with varying shell thicknesses as a function of temperature in various solvents: (a) water, (b) silicon oil, (c) toluene. The silica thicknesses are 0 nm (circle), 6 nm (triangle), 18 nm (square), and 38 nm (rhombus). (d) Temperature dependence of the Grüneisen parameter (left axis) for water (open circles) and toluene (open triangles) as well as the measured photoacoustic signal (right axis) of water (solid circle) and silicon oil (solid square). The error bar represents the standard error of 16 signals of 8 pulses each. Reprinted with permission from ref 94. Copyright 2011 John Wiley and Sons.

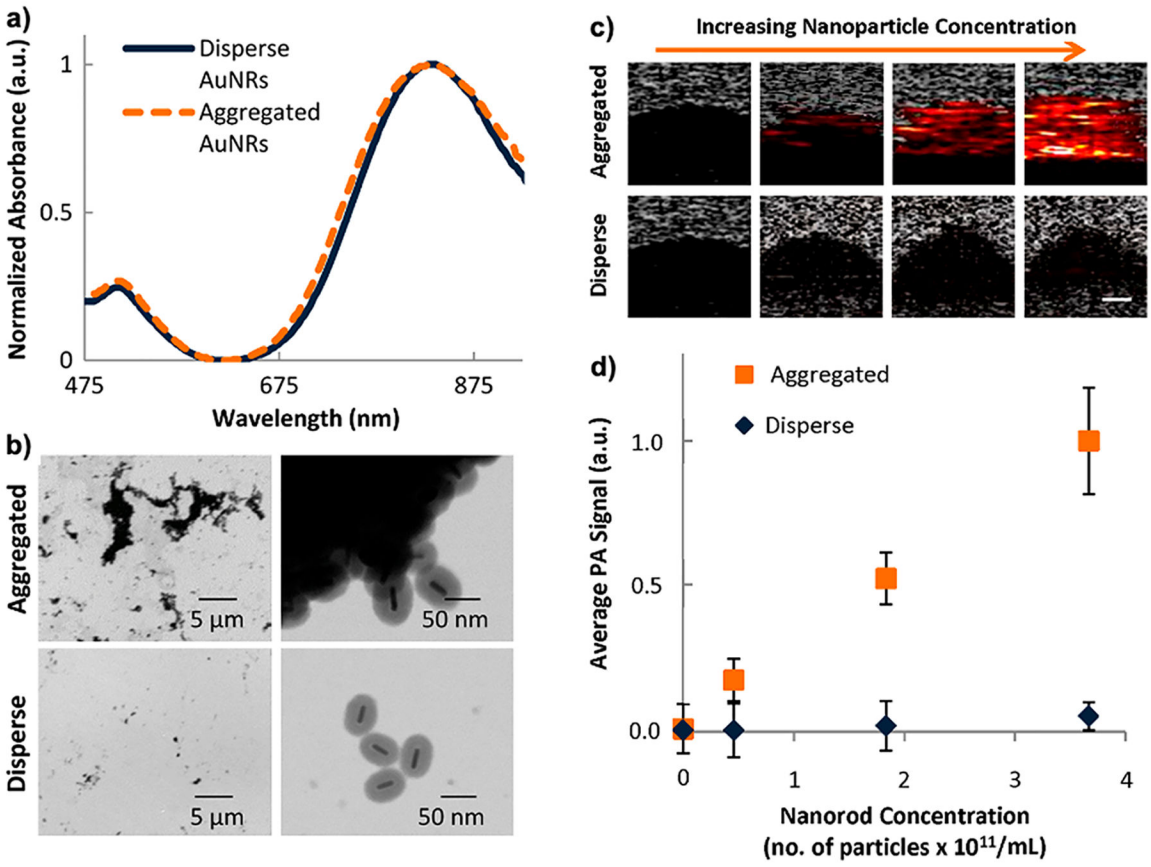

Figure 7.

Overlapping thermal profiles increase the rate of thermal flux into the solvent. (a) Absorption spectra of dispersed and aggregated silica-coated gold nanorods show no plasmon coupling between aggregates. (b) Transmission electron microscopy images confirming aggregation of particles. PA signal from aggregated silica-coated AuNRs is higher than that of the dispersed controls. (c) PA images corresponding to varying concentrations of nanoparticles. (d) Average PA signal as a function of nanorod concentration for aggregated and dispersed particles. Aggregation causes the thermal profiles of the nanoparticles to overlap, increasing the rate of heat flux into the solvent and hence enhancing PA. Reprinted with permission under a Creative Commons (BY 4.0) – Gold open access license from ref 102. Copyright 2013 International Society of Optics and Photonics (SPIE).